Palmitoylated Importin α Regulates Mitotic Spindle Orientation Through Interaction with NuMA

Authors

Patrick James Sutton[1,*], Natalie Mosqueda[1] and Christopher W. Brownlee[1,2]

Author Affiliations and Footnotes

[1]Department of Pharmacological Sciences, Stony Brook University; Stony Brook, 11794, United States of America.

[2]Lead Contact

*Correspondence: Patrick.Sutton@stonybrook.edu (P.J.S), Christopher.Brownlee@stonybrook.edu (C.W.B)

Abstract

Regulation of cell division orientation is a fundamental process critical to differentiation and tissue homeostasis. Microtubules emanating from the mitotic spindle pole bind a conserved complex of proteins at the cell cortex which orients the spindle and ultimately the cell division plane. Control of spindle orientation is of particular importance in developing tissues, such as the developing brain. Misorientation of the mitotic spindle and thus subsequent division plane misalignment can contribute to improper segregation of cell fate determinants in developing neuroblasts, leading to a rare neurological disorder known as microcephaly. We demonstrate that the nuclear transport protein importin α, when palmitoylated, plays a critical role in mitotic spindle orientation through localizing factors, such as NuMA, to the cell cortex. We also observe craniofacial developmental defects in *Xenopus laevis* when importin α palmitoylation is abrogated, including smaller head and brains, a hallmark of spindle misorientation and microcephaly. These findings characterize not only a role for importin α in spindle orientation, but also a broader role for importin α palmitoylation which has significance for many cellular processes.

Introduction

Mitotic spindle orientation is a fundamental cellular process which regulates cell division orientation, a crucial aspect of mitosis that when dysregulated can lead to uncontrolled asymmetric division and overproliferation, or developmental defects due to premature stem cell differentiation, depending on the cell type (Bergstralh and St Johnston, 2014; Bergstralh et al., 2017; Charnley et al., 2013; Finegan and Bergstralh, 2019). Neuronal development in particular is heavily reliant on properly oriented cell divisions to ensure the correct timing of neuron

differentiation, a process that when disturbed can result in severe defects, such as microcephaly (Razuvaeva et al., 2023; Higgins and Goldstein, 2010; Konno et al., 2008).

Mitotic spindle orientation is largely controlled by the anchoring of astral microtubules (aMTs) to the cell cortex in metaphase, and the pulling force generated by the dynein/dynactin motor complex on aMTs during anaphase (Kiyomitsu and Cheeseman, 2012; Kotak and Gönczy, 2013; Toyoshima and Nishida, 2007; Pietro et al., 2016; Bergstralh et al., 2017; Singh et al., 2021; Yang et al., 2014; Anjur-Dietrich et al., 2024). aMTs are anchored at the cortex by a conserved complex of proteins consisting of Gαi, which through myristylation is thought to associate with the plasma membrane (PM), Leucine-Glycine-Asparagine repeat containing protein (LGN), which binds to Gαi, and Nuclear Mitotic Apparatus (NuMA), which binds to LGN and dynein/dynactin, facilitating the strong pulling force on the aMTs necessary for maintenance of spindle orientation in metaphase (Higgins and Goldstein, 2010; Pietro et al., 2016; Camuglia et al., 2022; Kiyomitsu and Cheeseman, 2012; Fankhaenel et al., 2023; He et al., 2023; Kiyomitsu and Boerner, 2021; Zheng et al., 2013; Okumura et al., 2018; Pirovano et al., 2019; Du and Macara, 2004; Neville et al., 2022; Yu et al., 2000; Bowman et al., 2006; Carvalho et al., 2015; Anjur-Dietrich et al., 2024). While all of these factors play a role in aMT anchoring during metaphase, only NuMA and dynein/dynactin are required during anaphase to ensure the proper separation of chromatin to the poles (Bergstralh and St Johnston, 2014; Kotak et al., 2014; Seldin et al., 2013). Additionally, it has been shown that LGN and Gαi are only required for NuMA localization to the cell cortex during metaphase, not anaphase (Okumura et al., 2018; Kiyomitsu and Boerner, 2021). However, it remains unclear how these factors localize to the PM during metaphase and how this membrane localization is maintained there when it is believed that only a singly myristoylated Gαi is responsible for membrane association of the entire aMT

57 anchoring complex. Recently it has been demonstrated that a single dynein motor interacts with
58 each aMT, suggesting that only a single complex of Gai, LGN, NuMA, and dynein is present at
59 the cortex for each aMT. This highlights the need for this complex to be strongly associated with
60 the PM (Anjur-Dietrich et al., 2024). Furthermore, the necessity for a significant pulling force
61 towards the PM during metaphase to orient the mitotic spindle and during anaphase to facilitate
62 separation of chromatin to the poles suggests that an additional factor, which can associate with
63 the PM via multiple interaction points, may be involved in aMT anchoring.

64 Importin α is a highly conserved and abundant protein known for functioning as a
65 nuclear transport adapter in interphase and as a spindle assembly factor during mitosis through
66 its ability to bind Nuclear Localization Signal (NLS) sequence containing proteins (Takeda et al.,
67 2011; Oka and Yoneda, 2018; Goldfarb et al., 2004). However in recent years, a number of
68 proteomic screens for palmitoylated proteins utilizing a variety of biochemical methods and mass
69 spectrometry verification have identified human importin α-1 (KPNA2) as a target for
70 palmitoylation (Won and Martin, 2018; Thinon et al., 2018; Serwa et al., 2015; Mariscal et al.,
71 2020; Schelar and Liu, 2008; Zhou et al., 2019; Sobocinska et al., 2018). Palmitoylation is a
72 reversible and dynamic process which modifies proteins post translationally with palmitate lipids
73 allowing both diffusion and vesicle mediated transport of palmitoylated proteins to the PM
74 (Guan and Fierke, 2011). Additionally, recent work in *Xenopus laevis* (*X. laevis*) revealed that
75 importin α can be reversibly sequestered to the PM via palmitoylation of 4 key residues, 3 of
76 which are conserved in humans (Brownlee and Heald, 2019). This same study found that when
77 palmitoylated, importin α acts as an evolutionarily conserved cell-surface area-to-volume sensor
78 that coordinately scales nuclear and spindle size to cell size. Following this work, mass
79 spectrometry methods have confirmed palmitoylation of at least one residue in human KPNA2 in

80 addition to the 3 residues conserved from *X. laevis* importin α-1 (Zhou et al., 2019) and
81 palmitoylation prediction screens have identified additional cysteine residues in human KPNA2
82 likely to be palmitoylated with high confidence. These findings raise the intriguing possibility
83 that importin α may have roles other than as a nuclear import adapter upon palmitoylation
84 (Brownlee and Heald, 2019).

85 Due to the requirement of an exceedingly strong pulling force to drive orientation of the
86 spindle and chromatin separation to the poles, we hypothesize that palmitoylated importin α
87 could provide a sufficiently strong interaction with the PM to anchor aMTs in mitosis. Importin
88 α when modified with palmitate lipids at multiple residues would provide a significantly
89 increased membrane association compared to singly myristoylated Gαi and could increase the
90 membrane association of the aMT anchoring complex as a whole if bound to the factors
91 involved. Notably, NuMA as well as Discs Large (Dlg), another protein recently implicated in
92 spindle orientation (Bergstralh et al., 2016; Carvalho et al., 2015; Saadaoui et al., 2014; Schiller
93 and Bergstralh, 2021), contain strongly predicted NLS sequences suggesting importin α may be
94 responsible for their cellular localization through importin α-NLS binding. Previous literature
95 has also investigated the effects of deleting the NLS of NuMA and determined that NuMA's NLS
96 is required for its cortical localization (Okumura et al., 2018). Additionally, findings which
97 demonstrate that NuMA does not require LGN or Gαi to localize to the polar cortex during late
98 anaphase raise the intriguing possibility that palmitoylated importin α may play a role in
99 NuMA's mitotic localization (Okumura et al., 2018; Kiyomitsu and Boerner, 2021). We
100 hypothesize that palmitoylated importin α could bind NuMA's NLS in metaphase, transport it to
101 the PM and therefore be necessary for NuMA's localization in metaphase and early anaphase,
102 and sufficient for NuMA's localization during late anaphase.

103 A key factor driving protein localization and spindle formation in mitosis is a gradient of
104 RanGTP generated by the chromosome-tethered RanGEF, RCC1 (Kalab and Heald, 2008). In
105 interphase, the same localized concentration of RanGTP in the nucleus facilitates release of cargo
106 from importins for proper nuclear transport (Kalab and Heald, 2008; Ozugergin and Piekny,
107 2021). All of these processes are driven by the binding of RanGTP to importin β, which causes
108 the dissociation of importins and any bound cargo (Kalab and Heald, 2008; Oka and Yoneda,
109 2018). In mitosis, chromosomes are arranged during metaphase in such a manner that the
110 tethered RCC1 generates a high concentration of RanGTP at the midline of the cell, but a low
111 concentration of RanGTP towards the poles (Ems-McClung et al., 2020). The lack of RanGTP at
112 the polar cortex and the abundance of RanGTP at the lateral cortex during metaphase due to the
113 equatorial localization of the mitotic Ran gradient indicates that importin α can remain bound to
114 NLS containing cargo at the polar cortex exclusively. Importantly, this is where aMTs are
115 anchored and NuMA has been found to localize (Kiyomitsu and Cheeseman, 2012; Oka and
116 Yoneda, 2018; Chang et al., 2017; Kalab and Heald, 2008; Ems-McClung et al., 2020). This
117 suggests that the Ran gradient can regulate the localization of NLS containing proteins at the PM
118 and therefore restrict localization of NuMA to the polar cortex, through interaction with
119 palmitoylated importin α. Additionally, it has been shown that manipulation of the Ran gradient
120 disrupts spindle orientation and the localization of spindle orientation factors (Kiyomitsu and
121 Cheeseman, 2013).

122 In the present work we demonstrate that importin α when palmitoylated is a key regulator
123 of mitotic spindle orientation through localization of NuMA to the PM during metaphase and as
124 such palmitoylation of importin α is required for proper control of cell division orientation. We
125 show that palmitoylated importin α can localize throughout the PM in mitotic cells and that

126 palmitoylation of importin α is required for both proper spindle orientation and proper NuMA
127 localization in metaphase. While importin α localizes to the entire PM when palmitoylated (at
128 both the lateral and polar cortex), the accumulation of RanGTP near the metaphase plate would
129 preclude importin α binding to NuMA, leading to accumulation of NuMA specifically to the
130 polar cortex, where aMTs are anchored. We also explore the effects of importin α palmitoylation
131 disruption on neuronal development in *X. laevis* and observe microcephaly which can be rescued
132 upon forcing importin α to the PM independent of palmitoylation, further supporting that PM
133 localization of palmitoylated importin α is a key regulator of mitotic spindle orientation.
134

135 **Results**
136

137 **Importin α Localizes to The Mitotic Polar Cortex at Metaphase in a Palmitoylation-**
138 **Dependent, but Not Cargo-Dependent Manner**

139 Importin α has long been recognized for its role in spindle assembly during mitosis by
140 facilitating the transport of spindle assembly factors to the midline of the cell, where mitotic
141 spindles form (Kalab and Heald, 2008; Kaláb et al., 2006; Weaver and Walczak, 2015; Goldfarb
142 et al., 2004). Furthermore, it has been demonstrated to influence spindle orientation through
143 regulation of TPX2 activity (Guo et al., 2019). However, recent work has demonstrated in *X.*
144 *laevis* that importin α can be post translationally modified with palmitate lipids to drive PM
145 localization (Brownlee and Heald, 2019). These palmitoylation sites are conserved in human
146 importin α and additional palmitoylation sites have been confirmed by palmitoylation prediction
147 screens (Figure EV1A) and multiple mass spectrometry studies of global palmitoylated proteins
148 (Mariscal et al., 2020; Zhou et al., 2019; Won and Martin, 2018; Thinon et al., 2018; Serwa et al.,
149 2015; Sobocinska et al., 2018). Additionally, NLS prediction screens have shown an enrichment

150 of NLS containing proteins which localize to the PM and play a role in a variety of cellular
151 processes, including spindle orientation (Figure EV1B&C).This suggests that palmitoylated
152 importin α may be involved in mitotic cellular processes outside of spindle assembly at the PM
153 by binding NLS containing proteins and localizing them there.

154 We sought to investigate other possible roles of palmitoylated importin α in mitosis by
155 either increasing or decreasing levels of palmitoylated importin α, as well as inhibiting importin
156 α's ability to bind or release cargo. To manipulate palmitoylation of importin α, we targeted the
157 specific proteins responsible for palmitoylating and depalmitoylating importin α. Palmitoylation
158 is catalyzed by palmitoyl acyl transferases (PATs), which attach palmitoyl groups to serine or
159 cysteine residues, while depalmitoylation is carried out by acyl protein thioesterases (APTs)
160 which remove palmityl groups (Guan and Fierke, 2011). To modulate palmitoylation levels
161 specifically, we used small molecule inhibitors to target porcupine (PORCN), the serine PAT
162 responsible for palmitoylation of serine residues on importin α, and APT1, the APT responsible
163 for depalmitoylation of importin α (Brownlee and Heald, 2019). HCT116 colorectal cancer cells
164 were selected for this study due to their established role as a model system for both spindle
165 orientation and NuMA localization (Okumura et al., 2018; Tsuchiya et al., 2021).

166 We investigated the role of importin α in palmitoylation-mediated PM targeting using
167 HCT116 cells synchronized in metaphase and treated with either DMSO (control) or Wnt-C59, a
168 competitive inhibitor of PORCN (Proffitt et al., 2013). Wnt-C59 treatment would be expected to
169 result in a reduction in cellular palmitoylated importin α levels, leading to a decrease in the
170 population of importin α localized to the PM. Conversely, palmostatin treatment, which inhibits
171 APT1 (Dekker et al., 2010; Lin and Conibear, 2015), would be expected to result in an increase

172 in palmitoylated importin α levels, known as hyper-palmitoylation, which would increase the
173 population of importin α localized to the PM.

174 Mitotic importin α cellular localization was assessed after 1 hour in the respective drug
175 treatments, with cell boundaries determined by bright-field microscopy (Figure EV2A). In
176 DMSO control cells, importin α is observed localizing to centrosomes, near the assembling
177 spindles, and at the PM (Figure 1A). Notably, Wnt-C59 treatment resulted in a 6-fold decrease of
178 importin α signal at the PM and a concurrent enrichment of importin α signal in the cytoplasm
179 (Figure 1A-D), while palmostatin treatment did not alter importin α PM localization compared to
180 DMSO control treatment (Figure 1A-D). PM localization in DMSO control cells was confirmed
181 by western blot analysis of subcellular-fractioned HCT116 cells. HCT116 cells were metaphase
182 arrested and fractionated into 4 fractions: nuclear, cytoplasmic, organelles, and PM. The PM and
183 cytoplasmic fractions were analyzed by SDS-PAGE and immunoblotted for β-tubulin, as a
184 cytoplasmic marker, plasma membrane Ca^{2+} ATPase1 (PMCA1), as a PM marker, and importin
185 α. β-tubulin was detected only in the cytoplasmic fraction and PMCA1 was detected only in the
186 PM fraction demonstrating proper isolation of cellular fractions. However, importin α was
187 detected in both the cytoplasmic and PM fractions confirming our immunofluorescence findings
188 that importin α localizes to the PM in metaphase-arrested cells (Figure 1E). These results
189 collectively suggest that palmitoylation of importin α during metaphase is required for its proper
190 localization to the cortex.

191 The localization of importin α during metaphase was also analyzed in the presence of
192 drugs that disrupt its ability to bind and release cargo. Metaphase-arrested HCT116 cells were
193 treated with either ivermectin, a small molecule inhibitor that prevents the binding of importin α
194 to NLS containing cargoes (Wagstaff et al., 2012) or importazole, a small molecule inhibitor of

195 importin based nuclear transport that prevents RanGTP mediated release of cargo from importins
196 (Soderholm et al., 2011) (Figure 1A-D). We observed that in both importazole and ivermectin
197 treated cells, importin α remained unperturbed at the PM (Figure 1A-D). Notably, in all drug
198 treatments mitotic spindles were still formed properly despite disruption of importin α
199 palmitoylation or NLS cargo binding. Taken together, these results suggest importin α partitions
200 to the mitotic cortex via palmitoylation and does not require binding of NLS-containing cargoes
201 to localize to the PM.

202 It is noteworthy that we also observe alterations in chromatin size in metaphase cells
203 treated with our drug array. Specifically, palmostatin, importazole and ivermectin treatments
204 appear to induce larger, more condensed chromatin compared to that observed in DMSO or Wnt-
205 C59 treated cells. This is in line with what has previously been reported by Brownlee and Heald
206 in 2019 and Zhou et al. in 2023. Specifically, palmitoylated importin α has been shown to
207 regulate organelle size scaling (Brownlee and Heald, 2019) and chromatin size scaling (Zhou et
208 al., 2023).

209 **Importin α Palmitoylation and Cargo Binding Is Required for Proper Mitotic Spindle**
210 **Orientation**

211 We next sought to determine the effect of both disrupting importin α's ability to properly
212 bind NLS-containing cargo and importin α mislocalization on the orientation of the metaphase
213 mitotic spindle. HCT116 cells were metaphase-arrested and treated with DMSO, Wnt-C59,
214 palmostatin, importazole, ivermectin, or 2-bromopalmitate, a pan palmitoylation inhibitor (Lin
215 and Conibear, 2015). The angle of the metaphase spindle was then calculated using the relative
216 horizontal and vertical distances between the two spindle poles (Figure 1F). Mitotic spindles
217 were found to be misoriented in all treatments other than palmostatin relative to the DMSO-

218 treated control (Figure 1G & H). Interestingly, disruption of importin α palmitoylation (Wnt-C59
219 treatment), which was previously shown to alter mitotic importin α localization, and disruption
220 of importin α's ability to properly bind and release cargo (ivermectin and importazole treatments
221 respectively) both resulted in spindle misorientation. These data suggest that importin α
222 palmitoylation is required for proper spindle orientation, and spindle orientation is dependent
223 upon importin α binding of NLS-containing cargo.

224 To determine if the spindle misorientation phenotypes observed when HCT116 cells were
225 treated with palmitoylation disrupting drugs were specifically due to mislocalization of importin
226 α from the cell cortex, we constructed a plasmid containing importin α modified with a C-
227 terminal CaaX domain. Addition of the CaaX domain to importin α facilitates its cortical
228 localization through farnesylation, irrespective of its palmitoylation status (Figure EV3). Unlike
229 palmitoylation, farnesylation is irreversible, enabling CaaX-modified proteins to be directed to
230 the membrane and remain tethered there(Tang et al., 2009; Tamanoi et al., 2001). HCT116 cells
231 were transfected via nucleofection to express CaaX-modified importin α or an unmodified
232 importin α 24 hours prior to metaphase arrest and subsequent drug treatment with DMSO or
233 Wnt-C59. We observed that HCT116 cells overexpressing unmodified importin α exhibited
234 significantly misoriented spindle structures when treated with Wnt-C59 compared to DMSO
235 treatment (Figure 1J). However, HCT116 cells overexpressing CaaX-modified importin α did
236 not exhibit misorientation of spindle structures under the same conditions (Figure 1I and J),
237 therefore rescuing spindle misorientation in Wnt-C59 treatment. This suggests that the spindle
238 misorientation phenotypes observed when palmitoylation is disrupted are specifically due to
239 mislocalization of importin α to the mitotic cell cortex.

240 Several cancer cell lines have been shown to harbor various mutations which exacerbate
241 mitotic spindle orientation phenotypes (Chhabra and Booth, 2021). Therefore, we repeated the
242 previous spindle orientation experiment using an hTERT immortalized cell line, RPE-1, treated
243 with Wnt-C59 and palmostatin (Figure 1K). We again observed that Wnt-C59, but not
244 palmostatin treatment resulted in mitotic cells with significantly misoriented spindle structures
245 relative to the DMSO control (Figure 1L). This confirmed the findings in HCT116 cells and
246 further suggests that palmitoylation of importin α is required for proper mitotic spindle
247 orientation.

248 Previous research has indicated that cell shape and stretch play a role in determining the
249 axis of spindle orientation and, consequently, division orientation (Finegan and Bergstralh, 2019;
250 Charnley et al., 2013). While recent work has demonstrated that mechanical force applied to cells
251 through stretching has a more pronounced effect on spindle orientation (by directly influencing
252 NuMA localization) than cell shape (Tarannum et al., 2022), we sought to determine whether our
253 palmitoylation and importin function-disrupting drug array had an impact on mitotic cell shape.
254 We measured the circularity of 60 mitotic HCT 116 cells per drug treatment and observed that
255 there was no significant reduction in cell circularity in any of our drug treatments (Figure
256 EV2B). In fact, palmostatin-treated cells exhibited a slightly increased circularity compared to
257 DMSO treated cells (Figure EV2B). These findings confirm that the observed spindle
258 misorientation is not attributable to alterations in cell shape.

259 **Importin α Interacts with NuMA but not Dlg at the Metaphase Cell Cortex**

260 Mitotic spindle orientation in vertebrates is mediated through aMT anchoring at the cell
261 cortex via a conserved protein complex consisting of LGN, Gαi, NuMA and dynein/dynactin
262 (Bergstralh et al., 2017). Of these known spindle orientation proteins, only NuMA contains a

263 known NLS sequence, suggesting it may be a potential binding partner of importin α. To confirm
264 the interaction between importin α and NuMA, we performed immunoprecipitation of the
265 endogenous proteins from metaphase-arrested HCT116 cells treated with DMSO, Wnt-C59 and
266 palmostatin. Our results demonstrated that importin α and NuMA coprecipitated equally in all
267 drug treatment conditions (Figure 2A), confirming importin α and NuMA binding which is
268 unaffected by palmitoylation disruption.

269 To further investigate if importin α-NuMA interactions occur specifically at the mitotic
270 cortex, where aMTs are anchored, we employed a rolling amplification based proximity ligation
271 assay (PLA) (Alam, 2018). Additionally, we also probed for importin a-Dlg interactions at the
272 mitotic cortex using the same assay, as Dlg has been recently implicated in spindle orientation
273 (Schiller and Bergstralh, 2021; Saadaoui et al., 2014; Bergstralh et al., 2016), and contains a
274 predicted NLS sequence. Therefore, we also probed for importin α-Dlg interactions at the
275 mitotic cortex using the same assay. Importin α interaction with NuMA or Dlg was quantified by
276 measuring the number of PLA foci in 3 regions of interest at the polar cortex, lateral cortex, and
277 in the cytoplasm to determine where in the cell these proteins were interacting (Figure 2B). PLA
278 was performed on metaphase-arrested HCT116 cells in DMSO control, Wnt-C59 and
279 palmostatin treated conditions using specific antibodies to importin α and either NuMA or Dlg
280 (Figure 2C and E, respectively). The assay revealed that importin α and NuMA interact at the
281 polar cortex of DMSO treated metaphase cells, but not Wnt-C59 treated cells. Additionally,
282 importin α-NuMA interactions were found at both the polar and lateral cortices in palmostatin
283 treated cells (Figure 2D). Palmostatin treated cells also exhibited a marked enrichment of
284 importin α-NuMA interactions at the centrosomes and along spindle structures (Figure 2D)
285 suggesting that importin α could associate more strongly with NuMA when hyper-palmitoylated.

286 It is noteworthy that importin α and NuMA were only found to interact at the polar cortex in
287 control conditions as we have previously demonstrated that palmitoylated importin α localizes
288 throughout the mitotic PM at both the polar and lateral cortex (Figure 1A). This is to be
289 expected, as although importin α is present throughout the cortex, the presence of the RanGTP
290 gradient at the midline of the cell prevents importin α from binding or remaining bound to the
291 NLS of NuMA at the lateral cortex, limiting their interaction to the polar cortex where aMTs are
292 anchored.

293 When probing for importin α interaction with Dlg, we observed that while importin α
294 and Dlg were found to interact throughout the cytosol, this interaction was not enriched at any
295 specific cellular location and was not altered by Wnt-C59 or palmostatin treatment (Figure 2F).
296 These results collectively suggest that precise importin α palmitoylation levels are required to
297 maintain the importin α-NuMA interaction at the mitotic polar cortex and that importin α and
298 Dlg do not interact at the PM. A potential explanation for importin α interacting with NuMA
299 specifically and not Dlg is that these proteins contain distinct NLS sequences, such that NuMA
300 has a bipartite NLS while Dlg is predicted to have a monopartite NLS (Chang et al., 2017). It is
301 plausible that palmitoylated importin α, which would need to bind to these proteins in order to
302 localize them to the membrane, binds preferentially to some NLS containing cargo over others.

303 To further validate that the interaction between NuMA and importin α occurs at the polar
304 cortex in a palmitoylation dependent manner, we transfected HCT116 cells with either importin
305 α-mCherry-HA or importin α-mCherry-HA-CaaX. As before, we treated the cells with Wnt-C59,
306 arrested them in metaphase, and performed a PLA for NuMA and the transfected construct
307 (Figure 2G). We observed that cells transfected with the wild-type importin α construct treated
308 with Wnt-C59 (Figure 2H) exhibited a PLA foci distribution similar to endogenous importin a

309 expressing cells treated with Wnt-C59 (Figure 2C). Conversely, cells transfected with the
310 importin α-CaaX construct treated with Wnt-C59 displayed a PLA foci distribution more similar
311 to DMSO-treated cells, with a significant shift in foci from the cytoplasm to the polar cortex
312 compared to the wild-type transfected cells. This shift suggests a rescue of importin α-NuMA
313 interactions solely by forcing importin α to the PM (Figure 2H).

314 To account for potential differences in NuMA or importin α protein levels after drug
315 treatments, we performed a western blot and found that none of the treatments altered protein
316 levels in metaphase-arrested HCT116 cells (Figure 2I, J & K). Taken together, these results
317 suggest that importin α interacts with NuMA at the mitotic polar cortex in a palmitoylation-
318 dependent manner.

319 **NuMA and Dynein/Dynactin Localization During Metaphase is Dependent on NuMA**
320 **Binding to Palmitoylated Importin α**

321 It has previously been shown that deletion of NuMA's NLS causes mislocalization of
322 NuMA away from the polar cortex (Okumura et al., 2018). Based on this and our findings that
323 importin α palmitoylation is required for proper spindle orientation, we reasoned that importin α
324 may be driving NuMA's mitotic localization to the polar cortex through binding NuMA's NLS
325 and anchoring it to the PM. We therefore sought to determine how disruption of importin α
326 palmitoylation and its ability to properly bind and release cargo could affect NuMA's mitotic
327 localization.

328 Metaphase-arrested HCT116 cells expressing mClover-NuMA were treated with
329 palmitoylation and importin α cargo binding altering drugs and analyzed for NuMA localization
330 in metaphase (Figure 3A). NuMA intensity was measured at three cellular locations (polar
331 cortex, lateral cortex, and cytoplasm). To account for cell-to-cell differences in fluorescent

332 intensity these measurements were normalized by calculating the ratio of polar cortex/lateral
333 cortex, polar cortex/cytoplasm, and lateral cortex/cytoplasm fluorescent intensities. In the DMSO
334 control there is an enrichment of NuMA at the polar cortex over the lateral cortex which is
335 consistent with previously reported NuMA localization demonstrating that mClover-NuMA
336 expression has no impact on localization (Kiyomitsu and Boerner, 2021). It is worth noting that
337 while importin α localizes to the PM at both the lateral and polar cortices (Figure 1A), NuMA
338 only localizes to the polar cortex in control conditions (Figure 3A). This is expected as the
339 RanGTP gradient at the midline of the cell would prevent NLS containing cargo, such as NuMA,
340 from remaining bound to importin α at the lateral cortex. Strikingly, NuMA polar cortex
341 enrichment was lost in all drug conditions (Figure 3B). In Wnt-C59 and ivermectin treated cells,
342 NuMA localization shifts away from the polar cortex and is instead enriched in the cytoplasm
343 compared to the DMSO control (Figure 3C). In palmostatin and importazole treated cells, NuMA
344 localization was no longer enriched at the polar cortex, but rather localized throughout the
345 cortical membrane, including the lateral cortex (Figure 3D). This unexpected lateral cortex
346 localization when importin α is hyper-palmitoylated upon palmostatin treatment, or cannot
347 release cargo upon importazole treatment, suggests that importin α may be an upstream regulator
348 of proper NuMA localization at the polar cortex. The observed NuMA localization in
349 palmostatin-treated cells is of particular interest, as there was no significant spindle
350 misorientation observed under these conditions, yet NuMA mislocalizes nonetheless. We
351 hypothesize that the complete absence of NuMA at the cell cortex as observed in Wnt-C59
352 treated cells has a more pronounced effect on spindle misorientation than NuMA localizing to
353 both polar and lateral cortices, as seen in palmostatin-treated cells (Figure 3A). In the conditions
354 with no cortical NuMA, aMTs would not be anchored to the cell cortex at all, while in conditions

355 with NuMA present at both the polar and lateral cortices, aMTs would still anchor to the cortex
356 albeit without spatial regulation. These results of NuMA mislocalization upon palmitoylation and
357 importin α function disruption suggest that palmitoylated importin α membrane localization and
358 cargo binding is necessary for NuMA's localization and maintenance to the mitotic polar cortex.
359 As dynein/dynactin are known to associate with the aMT anchoring complex through
360 NuMA binding, and we have found that palmitoylated importin α is required for NuMA PM
361 localization, we investigated the impact of disrupting importin α palmitoylation on dynactin
362 localization in metaphase-arrested HCT116 cells. Metaphase-arrested cells were treated with
363 DMSO, Wnt-C59 or palmostatin as described previously. We visualized $p150^{Glued}$, the large
364 subunit of dynactin to analyze localization of dynein/dynactin (Figure 3E). Dynactin localization
365 was quantified using the same method employed for NuMA localization. We found that in
366 DMSO-treated control cells dynactin was enriched at the polar cortex relative to the lateral
367 cortex and was substantially localized to the cortex relative to the cytoplasm (Figure 3F-H). This
368 localization pattern closely resembles that of NuMA and was similarly disrupted by both Wnt-
369 C59 and palmostatin treatments, albeit in distinct manners. In Wnt-C59 treated cells, dynactin
370 exhibited a significant increase in the cytoplasm relative to the polar cortex (Figure 3G).
371 Conversely, in palmostatin-treated cells, dynactin showed a significant increase at the lateral
372 cortex relative to the polar cortex (Figure 3F). This pattern of mislocalization largely aligns with
373 that of NuMA, suggesting that palmitoylated importin α is driving NuMA-dynein/dynactin
374 localization to the polar cortex, facilitating aMT anchoring. Notably, unlike NuMA, dynactin did
375 not exhibit a significant enrichment at the lateral cortex relative to the cytoplasm in palmostatin-
376 treated cells (Figure 3H). This disparity in localization patterns could be attributed to various
377 factors that would preclude excess dynein/dynactin from accumulating at the lateral cortex,

378 where the number of aMTs is significantly lower compared to the polar cortex. Further
379 investigation is warranted to elucidate the underlying mechanisms responsible for this disparity.
380 Nevertheless, the overall pattern of misorientation when importin α palmitoylation is disrupted
381 strongly supports the role of palmitoylated importin α role in NuMA-dynein/dynactin
382 localization.

383 **Disruption of Importin α Palmitoylation Results in Microcephaly-Associated Phenotypes in**
384 ***X. laevis***

385 Having established the role of palmitoylated importin α in mitotic spindle orientation by
386 localizing NuMA to the polar cortex and maintaining it there, we subsequently sought to validate
387 these findings in vivo. Numerous centrosomal and mitotic spindle orientation defects have been
388 linked to microcephaly, as the resulting misorientation of cell division during brain development
389 leads to a depletion of neuroprogenitor cells, and consequently, total brain tissue at the
390 completion of development (Bergstralh and St Johnston, 2014). The African clawed frog
391 *Xenopus laevis* has been used extensively as a model system to study microcephaly and
392 developmental craniofacial abnormalities (Kennedy and Dickinson, 2014; Lasser et al., 2019;
393 Shantanam and MUELLER, 2018). *X. laevis* has also been heavily utilized in mitotic spindle
394 orientation studies exploring the roles of cell shape and stretch on NuMA localization and in turn
395 spindle orientation (Tarannum et al., 2022; Stooke-Vaughan et al., 2017) making it an ideal
396 system for the present study. Consequently, we utilized this model organism to determine
397 whether mislocalization of importin α at the PM and subsequent spindle misorientation might
398 lead to microcephaly or microcephaly-associated phenotypes. Leveraging our in vitro
399 observations, we analyzed the effects of disrupting mitotic spindle orientation by abrogating
400 importin α palmitoylation in the developing *X. laevis* model system.

401 *X. laevis* eggs were fertilized, placed in drug baths containing DMSO, Wnt-C59 or
402 palmostatin at approximately NF stage 24 and allowed to develop until NF stage 42 when
403 craniofacial measures can first be made (Figure 4A) (Kennedy and Dickinson, 2014; Shantanam
404 and MUELLER, 2018). Drug treated *X. laevis* embryos were assessed for craniofacial defects by
405 three metrics: distance between eyes, snout length and overall head area. Embryos were
406 immobilized in MS-222 and imaged from a dorsal perspective allowing for direct measurement
407 of cranial morphometrics. Both Wnt-C59 and palmostatin treatments significantly altered all
408 three metrics of head shape/size (Figure 4B) indicating that precise importin α palmitoylation is
409 required for proper craniofacial development in *X. laevis*. In addition to alterations in head shape,
410 drug treated tadpoles also exhibited other body morphology defects. Notably, Wnt-C59 treated
411 tadpoles exhibited much smaller tails than other conditions and a much higher mortality rate than
412 other conditions (Figure EV4).

413 While craniofacial abnormalities are a hallmark of microcephaly, we wanted to directly
414 measure potential microcephaly-associated phenotypes. We therefore sought to quantify the
415 neuroprogenitor population in the various drug treated *X. laevis* tadpoles. DMSO, Wnt-C59 and
416 palmostatin treated *X. laevis* embryos were analyzed at NF stage 46, when brain development
417 expansion reaches its apex (Exner and Willsey, 2021) by immunostaining for nestin, a
418 neuroprogenitor marker (Suzuki et al., 2010). Immunofluorescence images were taken of tadpole
419 forebrains and analyzed for the number of total cells, determined by DNA signal, that were
420 positive for nestin, indicating a neuroprogenitor identity (Figure 4C). Due to higher mortality
421 rate in Wnt-C59 treated *X. laevis* embryos, no Wnt-C59 treated tadpoles survived to NF stage 46
422 to be analyzed, indicative of severe developmental defects in both the brain and other tissue.
423 Palmostatin treated *X. laevis* embryos survived to NF stage 46 at the same rate as DMSO

424 controls but exhibited a significantly diminished neuroprogenitor population (Figure 4D). While
425 total cell count remained the same from DMSO to palmostatin treatments, the number of nestin
426 positive cells decreased (Figure 4D). This decrease in neuroprogenitors at NF stage 46 suggests
427 that the morphometric defects observed previously are indicative of true microcephaly, which is
428 characterized by defects in neuroprogenitor population maintenance.

429 To further characterize the observed microcephaly-associated phenotypes NF stage 42
430 drug treated *X. laevis* embryos were analyzed for the number of phosphohistone 3 (PH3) positive
431 cells, a marker for actively dividing cells (Elmaci et al., 2018), in the brain as a decrease in active
432 divisions of cells in the brain throughout development is a hallmark of microcephaly. Embryos
433 treated with DMSO or Wnt-C59 were wholemount immunostained for DNA and PH3 and
434 imaged via confocal microscopy to determine the number of cells positive for PH3 in the brain
435 (Figure 5A). Wnt-C59 treated embryos exhibited a 6-fold decrease in the number of actively
436 dividing cells compared to DMSO control conditions (Figure 5D). Additionally, Wnt-C59 treated
437 embryos at NF stage 42 displayed deformed brains which lacked mid and forebrain patterning.
438 These results together with our morphometric measurements indicate that dysregulation of
439 palmitoylation causes craniofacial defects and particularly microcephaly in developing *X. laevis*
440 embryos.

441 **Forcing Importin α to the PM Rescues *X. laevis* Microcephaly Phenotypes Observed When**
442 **Palmitoylation is Disrupted**

443 Up to this point we have exclusively altered importin α palmitoylation using small
444 molecule inhibitors, such as Wnt-C59 and palmostatin. Wnt-C59, however, exhibits off-target
445 effects by inhibiting the PAT PORCN, which palmitoylates Wnt for secretion in addition to
446 importin α. Given the crucial role of Wnt signaling in stemness and whole body development in

447 *X. laevis* (Yu et al., 2024), it is plausible that the observed effects in Wnt-C59-treated embryos
448 are off-target effects and cannot be directly attributed to importin α palmitoylation. Critically, to
449 address these off-target effects we investigated whether the loss of mitotic cells in the brain
450 leading to microcephaly was specifically caused by inhibiting importin α palmitoylation. To this
451 end, we utilized CaaX-modified importin α to force it to the cell membrane independently of
452 palmitoylation. Previously, we demonstrated that expression of CaaX-modified importin α could
453 rescue spindle misorientation phenotypes induced by Wnt-C59 treatment in human cell culture
454 (Figure 1E). By forcing importin α to the cell membrane while importin α palmitoylation is
455 abrogated, we can determine whether the microcephaly phenotype observed in Wnt-C59-treated
456 *X. laevis* embryos is specifically attributable to the absence of membrane-bound importin α or
457 other off-target effects.

458 We found that when *X. laevis* embryos were injected with CMV promoter-driven
459 wildtype and CaaX importin α they exhibited increased mortality and developmental defects
460 likely due to overexpression associated issues (Figure EV5). To combat this, an importin α-CaaX
461 construct was developed in a tetracycline inducible vector, pcDNA4TO, that would allow for
462 titratable levels of importin α expression. Additionally, we mitigated global developmental
463 defects of importin α overexpression by targeting expression exclusively to the D11 blastomere
464 of the developing embryo which is fated to give rise to the brain (Moody, 1987a; b*). X. laevis*
465 embryos were co-injected with importin α-CaaX pcDNA4TO and a plasmid expressing the tet
466 repressor at the D11 blastomere and analyzed for potential rescue of microcephaly (Figure 5B).

467 Importantly, *X. laevis* embryos microinjected with importin α-CaaX pcDNA4TO at the
468 D11 blastomere and treated with Wnt-C59 exhibited a rescue of PH3 levels in the brain at NF
469 stage 42 compared to uninjected Wnt-C59 treated embryos (Figure 5D). Additionally, the

470 microinjected tadpoles exhibited brain morphology more similar to the canonical brain
471 morphology at this stage, as seen in the DMSO control, than compared with the uninjected Wnt-
472 C59 treated embryos (Figure 5A&B). When treated with Wnt-C59, Importin α-CaaX injected
473 embryos showed brain PH3 levels about 2.5 times higher than both uninjected embryos and
474 embryos injected at D11 with an mCherry tagged CaaX domain (Figure 5C&D). Taken together,
475 these results suggest that disrupting importin α palmitoylation leads to a loss of dividing cells in
476 the developing *X. laevis* brain, which subsequently causes microcephaly. Furthermore, the
477 expression of the membrane-bound importin α CaaX construct, but not the uninjected, or
478 mCherry CaaX constructs, can rescue both brain cell proliferation and attenuate microcephaly in
479 *X. laevis* compared to drug treatment alone. This finding aligns with our in vitro work in cell
480 culture, where forcing importin α to the cell cortex was able to rescue spindle misorientation
481 (Figure 1I). These results demonstrate that the membrane localization of importin α is sufficient
482 to rescue palmitoylation disruption-induced spindle misorientation in vitro and microcephaly in
483 vivo.
484

485 **Discussion**

486 Importin α is primarily recognized as a nuclear transport protein during interphase and as
487 a spindle assembly factor in mitosis by binding NLS sequence-containing proteins. In interphase,
488 importin α binds to NLS sequence containing proteins and transports them into the nucleus,
489 while in mitosis importin α binds to NLS sequence-containing proteins and transports them to
490 the developing spindles at the midline of the cell (Takeda et al., 2011; Oka and Yoneda, 2018;
491 Goldfarb et al., 2004). In the present study we have demonstrated a previously uncharacterized
492 role for importin α at the PM. We have shown that importin α, when partitioned to the PM via

493 palmitoylation, plays a crucial role in mitotic spindle orientation. Disruption of importin α
494 palmitoylation resulted in mitotic spindle misorientation and mislocalization of the aMT
495 anchoring protein NuMA. While LGN and Gαi are necessary to ensure proper spindle
496 orientation in metaphase (Bergstralh et al., 2017; Neville et al., 2022; Zhong et al., 2022), we
497 have shown that importin α, while palmitoylated, is also required for proper NuMA localization
498 and in turn proper spindle orientation, irrespective of LGN and Gαi. Our finding that importin α
499 plays a role in spindle orientation through interaction with the aMT anchoring complex is
500 especially noteworthy in that importin α's ability to bind cargo is sensitive to the RanGTP
501 gradient which emanates from the chromatin. As NuMA is a known cargo of importin α and has
502 been shown in this work to interact with palmitoylated importin α at the polar cortex, this
503 provides a regulatory pathway by which the localization of the chromatin and the RanGTP
504 gradient can determine where aMTs are anchored. This relationship is able to explain the well-
505 defined spatial organization of the aMT anchoring complex exclusively to the polar cortex which
506 has been shown to be essential for proper spindle orientation (Bergstralh et al., 2017)(Figure 6).
507 Our results demonstrated that disruption of importin α palmitoylation leads to
508 developmental defects in *X. laevis* embryos, specifically microcephaly. Defects in neurogenesis,
509 in particular microcephaly, have long been linked to spindle misorientation(Taverna et al., 2014).
510 Neuroprogenitors rely on proper spindle orientation to correctly align polarity cues which
511 regulate cell fate determination in the developing brain (Taverna et al., 2014). During early
512 neurogenesis, neuroprogenitors rely on several symmetric divisions to generate a large enough
513 population of cells to later divide asymmetrically and differentiate into neurons. Spindle
514 misorientation can cause neuroprogenitors to prematurely differentiate, depleting the pool of
515 neuroprogenitors, resulting in an overall decrease in neuronal tissue and microcephaly (Taverna

516 et al., 2014; Razuvaeva et al., 2023). Expression of importin α modified with a CaaX motif,
517 which is forced to the PM by farnesylation, effectively rescued both the spindle misorientation
518 observed in HCT116 cells and the developmental defects observed in *X. laevis* embryos. These
519 findings further emphasize the role of palmitoylated importin α in spindle orientation and
520 neurogenesis. The observed rescues not only demonstrate importin α's involvement in aMT
521 anchoring, but also that the spindle misorientation and microcephaly observed when
522 palmitoylation was disrupted by Wnt-C59 treatment are not due to off-target effects and can be
523 attributed, in part, to mislocalization of importin α from the PM, as those phenotypes are
524 reversed by forcing importin α to the PM.

525 We propose an updated model for mitotic spindle orientation in which aMT anchoring at
526 the cell cortex is mediated by palmitoylated importin α through its interaction with NuMA
527 (Figure 6). In this newly proposed model, the RanGTP gradient plays a significant role in
528 limiting the binding of NuMA to palmitoylated importin α to the polar cortex exclusively. This
529 provides a mechanism by which palmitoylated importin α can regulate spindle orientation by
530 binding directly to NuMA with spatial binding cues provided by the RanGTP gradient emanating
531 from the chromosomes at the metaphase plate (Figure 6). Notably, our newly proposed model
532 provides a mechanistic link between factors known to affect spindle orientation, such as cell size,
533 shape, and stretch, and the localization of aMT anchoring proteins. Given that palmitoylated
534 importin α and its interaction with RanGTP is essential for proper localization of the aMT
535 anchoring complex, these factors known to affect spindle orientation must exert their influence,
536 at least in part, through palmitoylated importin α. Further studies to explore NuMA activation
537 via phosphorylation, which has been previously linked with NuMA PM localization and
538 association with the aMT anchoring complex of proteins (Gallini et al., 2016), and its impact on

binding to palmitoylated importin α would be beneficial to expand this model and provide a robust view of NuMA localization in mitosis. It is reasonable to hypothesize that phosphorylated NuMA could bind with differential preference to palmitoylated importin α similar to our observation that hyper-palmitoylation of importin α increased NuMA/importin α interaction, but this warrants further study and remains speculative.

The present work not only highlights the importance of importin α as a key upstream regulator in mitotic spindle orientation, but also serves as the first evidence of a novel protein transport pathway by which palmitoylated importin α can transport NLS containing proteins to the PM. This new transport pathway could be involved in several cellular processes due to the abundance of NLS containing proteins that enrich at the PM and provides a potential new level of regulation of these processes through regulation of importin α palmitoylation. Overall, our work challenges the long-standing dogma of importin α only facilitating transport into the nucleus and suggests that there are a number of potential non-canonical roles for importin α at the membrane.

Acknowledgements

We thank Natalie Mosqueda, Kathryn Malone, and Melanie Garcia for their constructive feedback on this work, engaging discussions, and edits during the writing of this manuscript. We thank Maurice Kernan, Holly Colognato, Gerald Thomsen, and Daniel Levy for their insights and suggestions on experimental approach. We thank the Stony Brook University Central Microscopy Imaging Center (CMIC) and Guowei Tian for assistance in imaging with Zeiss LSM 980 Airsycan 2 NLO Two-Photon Confocal Microscope. Work was supported by National Institutes of Health grant 1R35GM147569-01 (C.W.B).

562

563 **Author Contributions**

564 C.W.B initially conceptualized the project. P.J.S and C.W.B designed the project. P.J.S performed
565 the majority of experiments and all analysis of data. N.M performed co-immunoprecipitation
566 experiments. P.J.S prepared the figures, and P.J.S and C.W.B wrote the manuscript. P.J.S, C.W.B
567 and N.M edited and revised the manuscript. C.W.B procured funding for this project.

568

569 **Declaration of Interests**

570 The authors declare no competing interests.

571

572 **Figures**

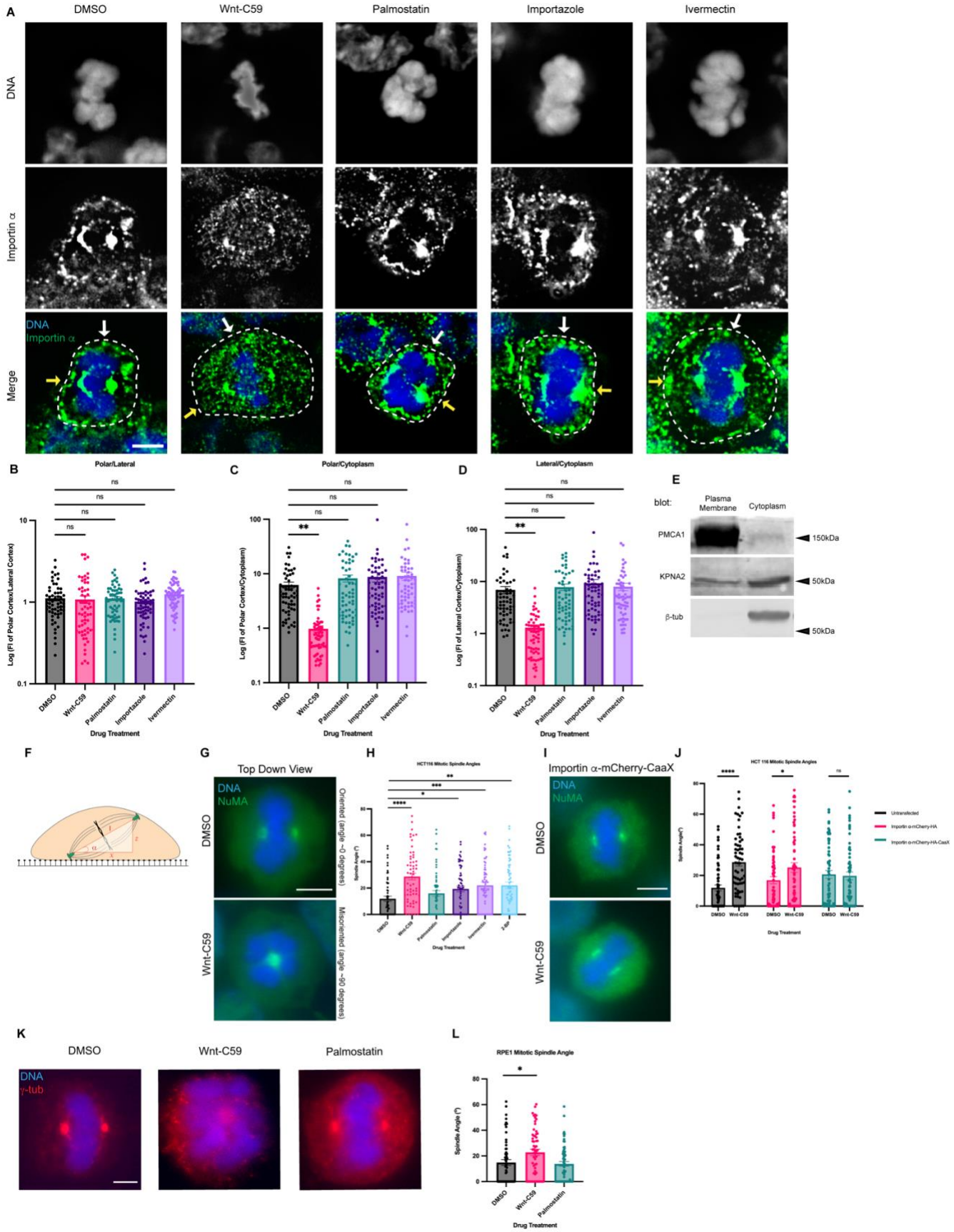
A
DMSO
Wnt-C59
Palmostatin
Importazole
Ivermectin
DNA
Importin α
Merge
DNA
Importin α
B
Polar/Lateral
Log (FI of Polar Cortex/Lateral Cortex)
Drug Treatment
C
Polar/Cytoplasm
Log (FI of Polar Cortex/Cytoplasm)
D
Lateral/Cytoplasm
Log (FI of Lateral Cortex/Cytoplasm)
E
blot:
Plasma Membrane
Cytoplasm
PMCA1
KPNA2
β-tub
150kDa
50kDa
50kDa
F
G
Top Down View
DNA
NuMA
DMSO
Wnt-C59
Oriented (angle ~0 degrees)
Misoriented (angle ~90 degrees)
H
HCT116 Mitotic Spindle Angles
Spindle Angle (°)
Drug Treatment
I
Importin α-mCherry-CaaX
DNA
NuMA
DMSO
Wnt-C59
J
HCT 116 Mitotic Spindle Angles
Spindle Angle(°)
Drug Treatment
Untransfected
Importin α-mCherry-HA
Importin α-mCherry-HA-CaaX
K
DMSO
Wnt-C59
Palmostatin
DNA
γ-tub
L
RPE1 Mitotic Spindle Angle
Spindle Angle (°)
Drug Treatment

573

574 **Figure 1. Palmitoylation Mediated Cortical Localization of Importin α and Importin α**
575 **Cargo Binding are Required for Proper Mitotic Spindle Orientation.**
576 A) Immunofluorescence images of importin α localization in metaphase-arrested (refer to
577 Materials & Methods) HCT116 cells incubated for 1 hour with DMSO, drugs that inhibit
578 importin palmitoylation (10μM Wnt-C59) drugs that enhance importin palmitoylation (50μM
579 palmostatin), and drugs that inhibit importin cargo binding (25μM ivermectin) or cargo release
580 (40μM importazole). Yellow arrows indicate cortical poles and white arrows indicate lateral
581 cortex. Scale bar=5μm. Cell boundaries determined by brightfield.
582 B-D) Quantification of importin α localization in drug treated cells. Measurements of importin
583 α signal intensity were made at three cellular locations: polar cortex, lateral cortex and
584 cytoplasm. Polar cortex measurements were made for each cell at the pole with the higher
585 measure of intensity, a similar method was used for lateral cortex measurements and cytoplasm
586 measurements were made at the midline of the cell. These measurements were normalized to
587 each other on a cell-by-cell basis by determining the ratio of cortical vs lateral importin α,
588 cortical vs cytosolic importin α, and lateral vs cytosolic importin α. Mean +/- SEM n=60 from 2
589 replicates **=$p<0.01$ determined by Student's t-test.
590 E) Western blot of HCT116 cell fractions following subcellular fractionation to separate PM,
591 cytoplasmic, organelle, and nuclear fractions. PM and cytoplasmic fractions shown. Western
592 blots were immunostained for PMCA1 (PM marker), β-tubulin (cytoplasmic marker), and
593 importin α (KPNA2).
594 F) Cartoon representation of a metaphase cell with misoriented spindles mounted on a coverslip
595 indicating the angle, α, which was measured as the arctangent of the horizontal distance, z, over

596 the vertical distance, x, between the two centrosomes to determine the angle of spindle
597 structures.
598 G) Immunofluorescence images of metaphase-arrested HCT116 cells in presence of DMSO or
599 10μM Wnt-C59 stained for NuMA. DMSO treated cell represents a properly oriented cell with a
600 spindle angle of 0 degrees relative to the parallel of the coverslip the cells were mounted on.
601 Wnt-C59 treated cell represents a severely misoriented cell with a spindle angle of 90 degrees
602 relative to the parallel of the coverslip the cells were mounted on. Scale bar=5μm
603 H) Quantification of mitotic spindle angles for metaphase-arrested HCT116 cells incubated in
604 DMSO, 10μM Wnt-C59, 50μM palmostatin, 40μM importazole, 25μM ivermectin, or 100μM 2-
605 bromopalmitate for 1 hour prior to analysis. All drug treatments except palmostatin significantly
606 increased the mean spindle angle of metaphase cells relative to a DMSO control. Mean +/- SEM,
607 n=60 mitotic cells from 2 replicates *=p<0.05 **=p<0.01 ***=p<0.001 ****=p<0.0001
608 determined by Student's t-test. Refer to Materials & Methods for method of determining spindle
609 angle.
610 I) Immunofluorescence images of metaphase-arrested HCT116 cells transfected via
611 nucleofection with importin α-mCherry-HA-CaaX and incubated in either DMSO or 10μM Wnt-
612 C59 for 1 hour prior to analysis stained for NuMA. Scale bar=5μm.
613 J) Quantification of mitotic spindle angles for metaphase-arrested HCT116 cells incubated with
614 DMSO or 10μM Wnt-C59 expressing importin α-mCherry-HA or importin α-mCherry-HA-
615 CaaX. Cells expressing importin α-mCherry-HA-CaaX showed no spindle misorientation when
616 treated with Wnt-C59. Mean +/- SEM, n=60 mitotic cells from 2 replicates *=p<0.05
617 ****=p<0.0001 determined by Student's t-test.

618 K) Immunofluorescence images of metaphase-arrested RPE-1 cells incubated with DMSO,
619 10μM Wnt-C59, or 50μM palmostatin for 1 hour prior to analysis stained for γ-tubulin. DMSO
620 treated cells are representative of cells with properly oriented spindles. Wnt-C59 treated cells
621 were significantly misoriented and palmostatin treated cells were properly oriented when
622 compared to DMSO control. Scale bar=5μm
623 L) Quantification of mitotic spindle angles for metaphase-arrested RPE-1 cells incubated with
624 DMSO, 10μM Wnt-C59 or 50μM palmostatin for 1 hour prior to analysis. Wnt-C59 treatment
625 significantly increased the mean spindle angle of metaphase cells relative to a DMSO control
626 while palmostatin treatment did not significantly increase the mean spindle angle relative to a
627 DMSO control. Mean +/- SEM, n=60 mitotic cells from 2 replicates *=$p<0.05$ determined by
628 Student's t-test.
629

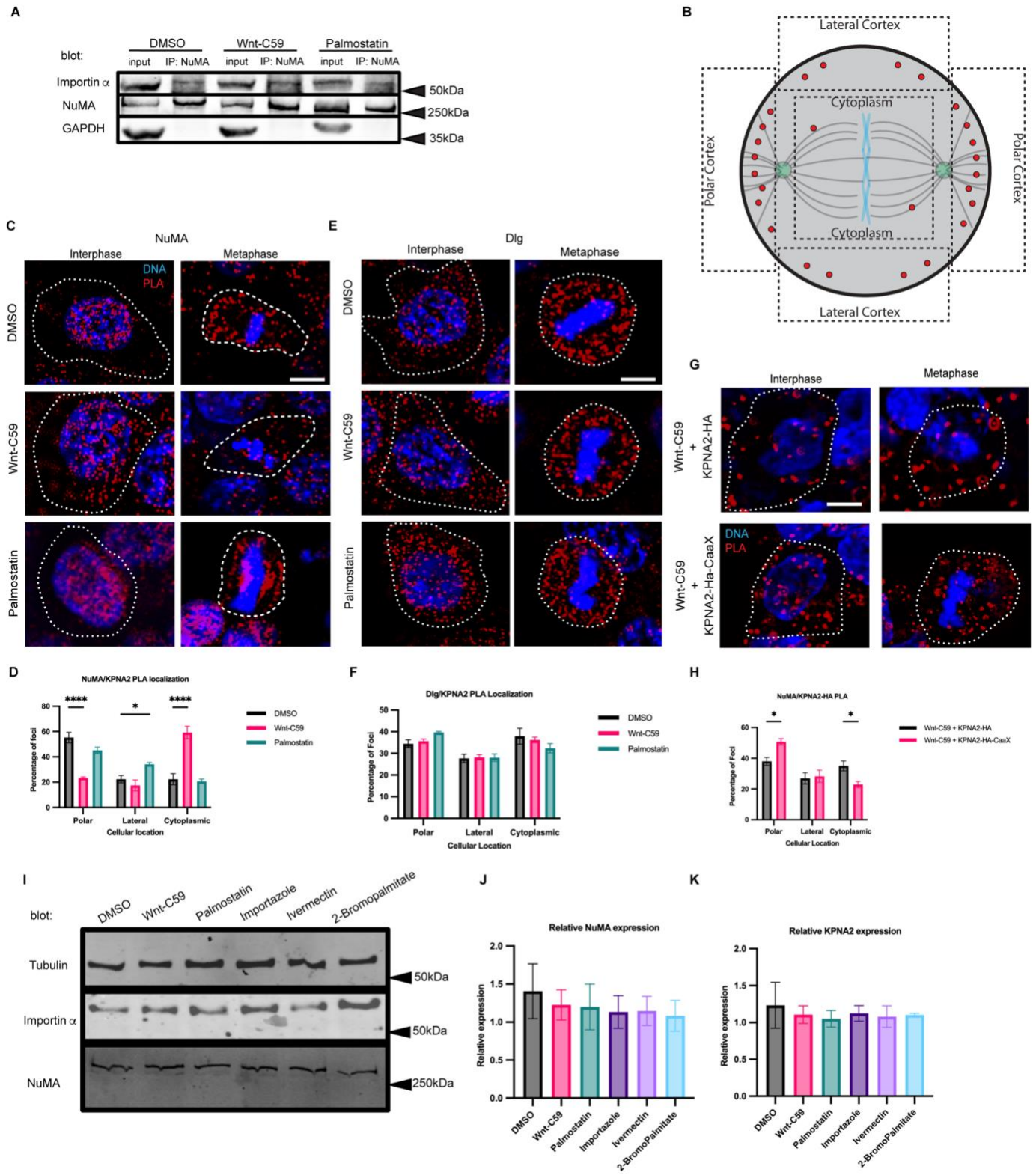

Figure 2. Importin α Interacts with NuMA, but not Dlg at the Metaphase Cell Cortex in a Palmitoylation Dependent Manner.

633 A) Western blot of NuMA immunoprecipitation from HCT116 cells treated with DMSO, 10μM
634 Wnt-C59 or 50μM palmostatin for 1 hour prior to analysis. Immunoprecipitation of NuMA
635 followed by importin α and NuMA western blot.
636 B) Schematic of PLA quantification. ROIs of quantification represented by dashed lines.
637 C) Immunofluorescence images of DuoLink proximity ligation assay (PLA) probing interaction
638 of NuMA with importin α (KPNA2) in interphase and metaphase-arrested HCT116 cells in the
639 presence of DMSO, 10μM Wnt-C59 or 50μM palmostatin for 1 hour prior to analysis. White
640 dashed lines indicate cell borders as determined by brightfield images. Scale bar=5μm.
641 D) Quantification of the percentage of importin α (KPNA2)-NuMA PLA foci at the polar cortex,
642 lateral cortex and cytoplasm in DMSO, Wnt-C59 and palmostatin-treated cells. Foci were
643 enriched at the polar cortex in DMSO treated cells, the cytoplasm in Wnt-C59 treated cells, and
644 the lateral cortex in palmostatin treated cells. Mean +/- SEM, n>136 foci *=p<0.05
645 ****=p<0.0001 determined by Student's t-test.
646 E) Immunofluorescence images of DuoLink PLA probing interaction of Dlg with importin α
647 (KPNA2) in interphase and metaphase-arrested HCT116 cells in the presence of DMSO, 10μM
648 Wnt-C59 or 50μM palmostatin. White dashed lines indicate cell borders. Scale bar=5μm.
649 F) Quantification of the percentage of importin α (KPNA2)-Dlg PLA foci at the polar cortex,
650 lateral cortex and cytoplasm in DMSO, Wnt-C59 and palmostatin treated cells. Localization of
651 PLA foci did not change across three drug treatments. Mean +/- SEM, n>297 foci, all data points
652 are non-significant as determined by Student's t-test.
653 G) Immunofluorescence images of DuoLink proximity ligation assay probing interaction of
654 NuMA with nucleofected importin α constructs (KPNA2-HA-mCherry and KPNA2-HA-
655 mCherry-CaaX) in interphase and metaphase-arrested HCT116 cells in the presence of DMSO or

656 10μM Wnt-C59 for 1 hour prior to analysis. White dashed lines indicate cell borders as
657 determined by brightfield images. Scale bar=5μm.
658 H) Quantification of the percentage of nucleofected importin α constructs(KPNA2)-NuMA PLA
659 foci at the polar cortex, lateral cortex and cytoplasm in Wnt-C59 treated cells. Cells nucleofected
660 with KPNA2-HA and treated with Wnt-C59 did not exhibit enrichment of foci at the PM and
661 instead showed foci throughout the cell. Cells nucleofected with KPNA2-HA-CaaX and treated
662 with Wnt-C59 exhibited foci enrichment at the PM indicating that expression of KPNA2-HA-
663 CaaX rescued the effects of Wnt-C59 treatment. Mean +/- SEM, n>195 foci *=p<0.05
664 determined by Student's t-test.
665 I) Western blot of importin α, NuMA and β-tubulin in metaphase-arrested HCT116 cells in the
666 presence of DMSO, 10μM Wnt-C59, 50μM Palmostatin, 40μM importazole, 25μM ivermectin,
667 or 100μM 2-bromopalmitate.
668 J and K) Quantification of NuMA and importin α (KPNA2) expression levels respectively,
669 relative to β-tubulin protein levels for each condition.
670

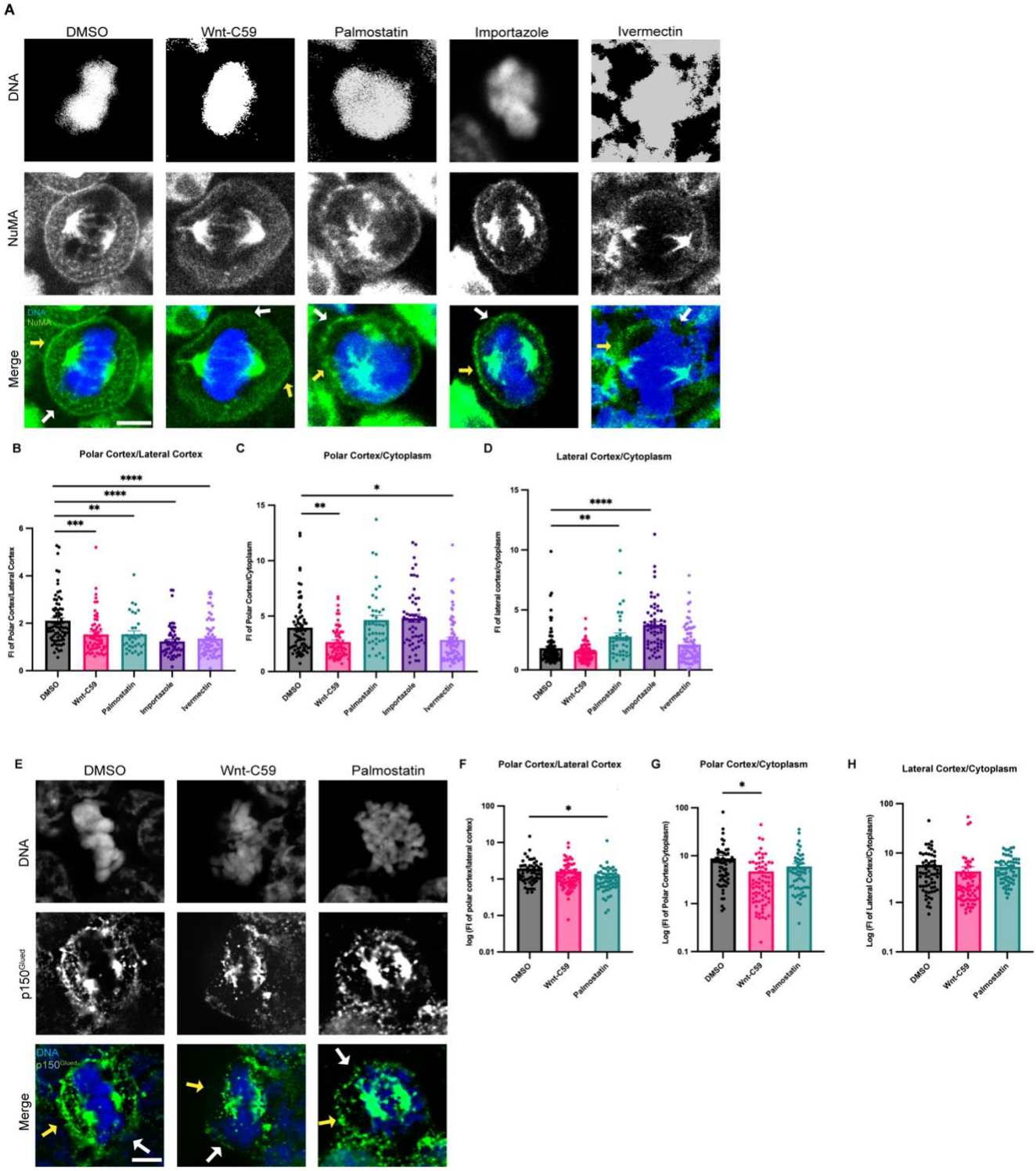

671

672 **Figure 3. Palmitoylated Importin α Regulates Cortical Localization of NuMA and**

673 **Dynein/Dynactin in Metaphase.**

674 A) Confocal images of NuMA localization in metaphase-arrested HCT116 cells in the presence
675 of DMSO, 10μM Wnt-C59, 50μM palmostatin, 40μM importazole or 25μM ivermectin. Yellow
676 arrows indicate cortical poles and white arrows indicate lateral cortex. Scale bar=5μm.
677 B-D) Quantification of NuMA localization in drug treated cells. Measurements of NuMA signal
678 intensity were made at three cellular locations: polar cortex, lateral cortex and cytoplasm. Polar
679 cortex measurements were made for each cell at the pole with the higher measure of intensity, a
680 similar method was used for lateral cortex measurements and cytoplasm measurements were
681 made at the midline of the cell. These measurements were normalized on a cell-by-cell basis by
682 determining the ratio of polar vs lateral NuMA, polar vs cytosolic NuMA, and lateral vs
683 cytosolic NuMA. Mean +/- SEM n>40 *=p<0.05 **=p<0.01 ***=p<0.001 ****=p<0.0001
684 determined by Student's t-test.
685 E) Immunofluorescence images of $p150^{Glued}$ localization in metaphase-arrested HCT116 cells
686 treated with either DMSO, 10μM Wnt-C59, or 50μM palmostatin. Yellow arrows indicate
687 cortical poles and white arrows indicate lateral cortex. Scale bar=5μm.
688 F-H) Quantification of $p150^{Glued}$ localization in drug-treated cells. Measurements of $p150^{Glued}$
689 signal intensity were made at three cellular locations: polar cortex, lateral cortex and cytoplasm.
690 Polar cortex measurements were made for each cell at the pole with the higher measure of
691 intensity, the same method being used for lateral cortex measurements and cytoplasm
692 measurements at the midline of the cell. These measurements were normalized on a cell-by-cell
693 basis by determining the ratio of polar vs lateral $p150^{Glued}$, polar vs cytosolic $p150^{Glued}$, and
694 lateral vs cytosolic $p150^{Glued}$. Mean +/- SEM n=60 *=p<0.05 determined by Student's t-test.
695
696

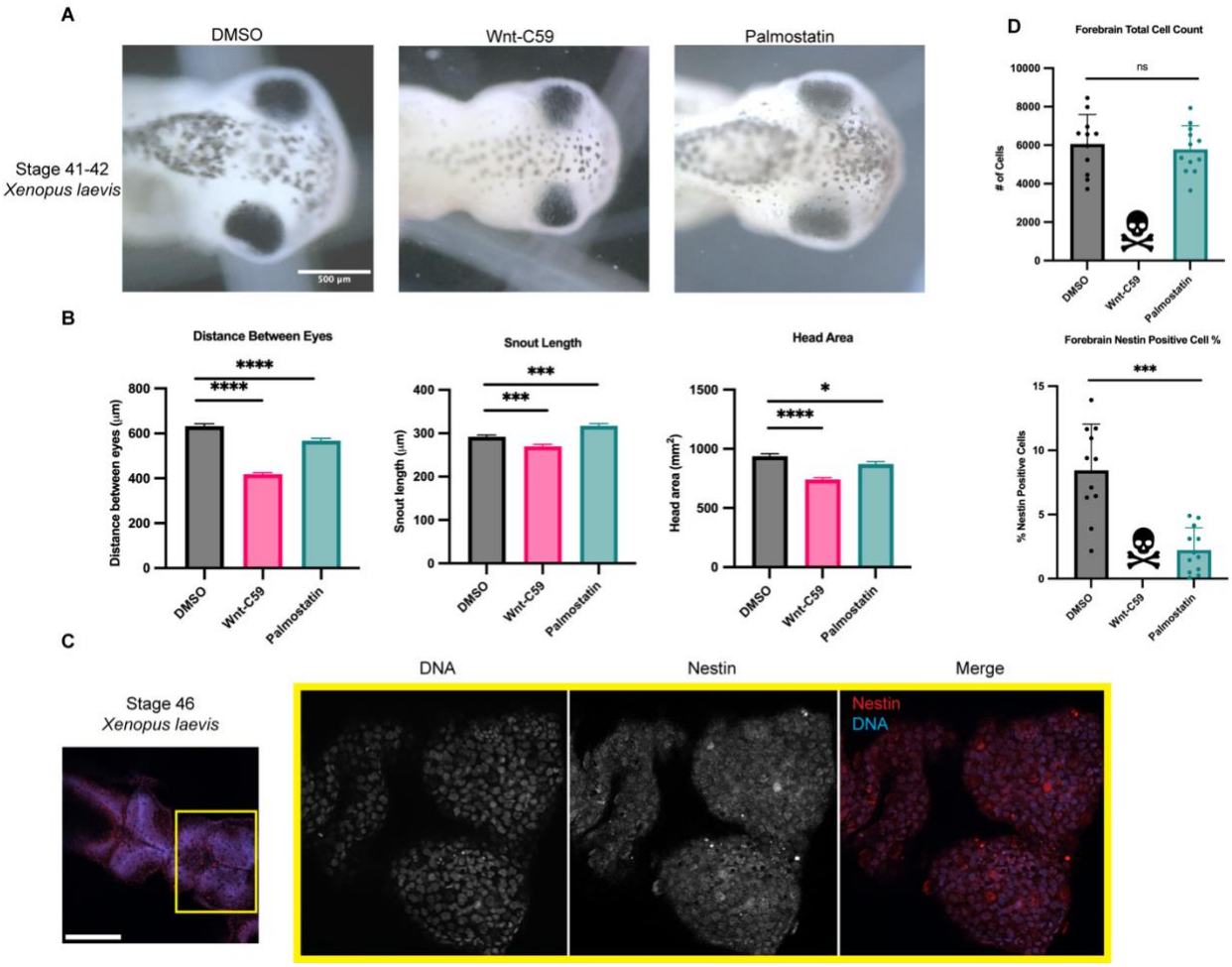

Figure 4. Regulation of Palmitoylation is Required for Proper Brain Development in *Xenopus laevis*.

A) Bright field images of NF stage 42 *X. laevis* grown in the presence of DMSO, 100µM Wnt-C59 or 1mM palmostatin. Scale bar=500µm

B) Measurements of drug treated stage 42 *X. laevis* head shape by 3 metrics: distance between eyes, snout length, and overall head area. All 3 metrics of head shape were significantly altered from DMSO control in both Wnt-C59 and palmostatin treatments. Mean +/- SEM n>55 *=p<0.05 ***=p<0.001 ****=p<0.0001 determined by Student's t-test.

C) Immunofluorescence images of DMSO treated NF stage 46 *X. laevis* immunostained for the neuroprogenitor marker nestin and stained with Hoechst to visualize DNA. Scale bar=250µm.

708 D) Quantification of total cell count in forebrains and percentage of forebrain cells positive for
709 nestin signal in NF stage 46 *X. laevis* grown in the presence of DMSO, 100μM Wnt-C59 or
710 1mM palmostatin. Quantifications were performed on maximum projection images from z-stack
711 images of *X. laevis* brains with a parent-child analysis to determine the number of total cells as
712 determined by Hoechst signal that also were positive for nestin signal. All Wnt-C59 treated *X.*
713 *laevis* embryos died before reaching NF stage 46 while all palmostatin treated *X. laevis* display a
714 significantly reduced neuroprogenitor population by nestin positive cell count. Mean +/- SEM
715 n=12 ***=$p<0.001$ determined by Student's t-test.
716

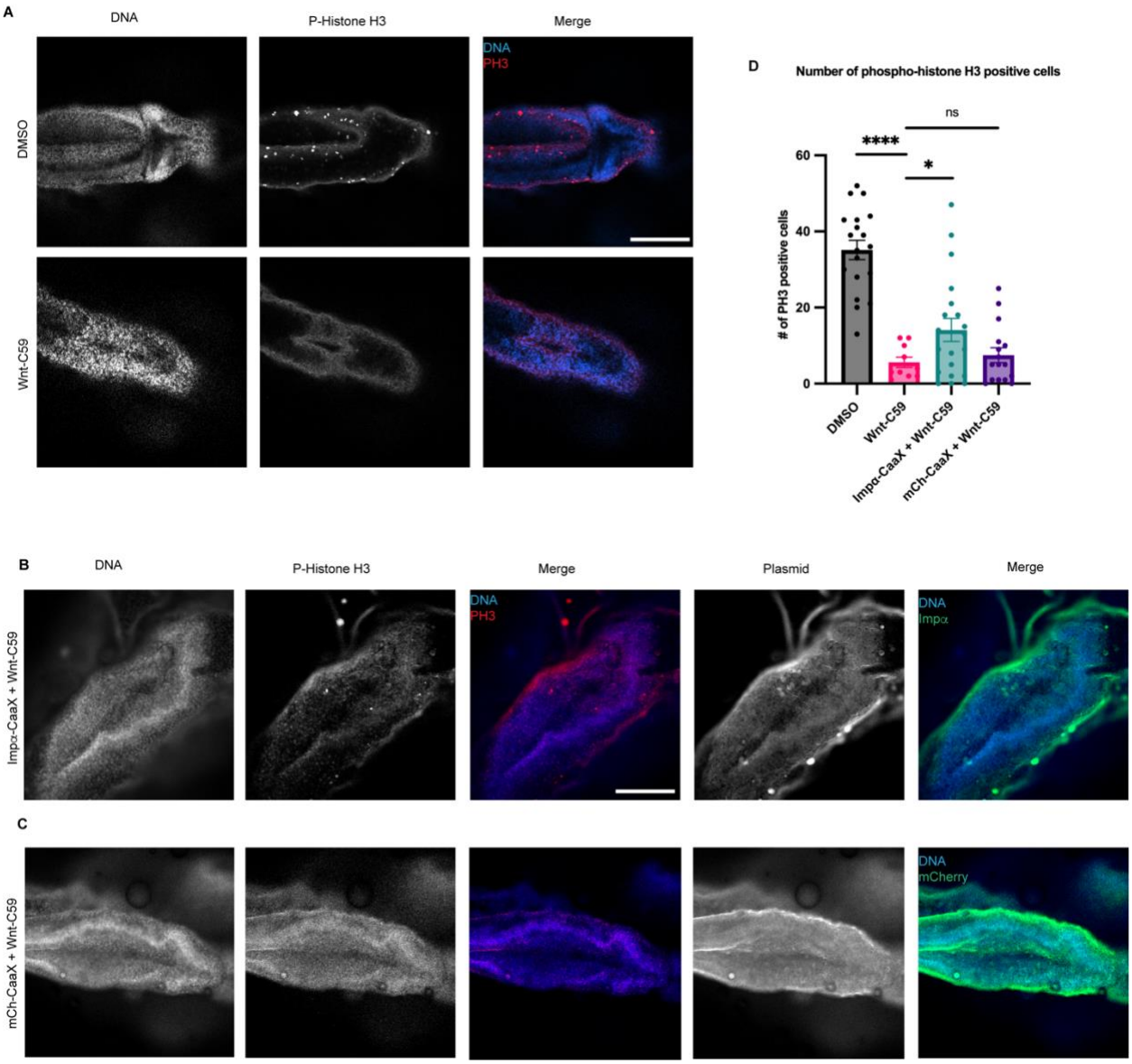

Figure 5. Overexpression of CaaX Modified Importin α in the Developing *X. laevis* Brain Partially Rescues Developmental Defects due to PORCN Inhibition.

A) Confocal images of NF stage 42 *X. laevis* brains from *X. laevis* grown in the presence of DMSO or 100μM Wnt-C59 immunostained for phospho-histone H3, a marker of actively dividing cells. Scale bar = 250μm.

B) Confocal images of NF stage 42 *X. laevis* brains from *X. laevis* expressing importin α modified with a c-terminal CaaX domain which forces cortical localization via farnesylation and

725 grown in the presence of 100μM Wnt-C59 immunostained for phospho-histone H3 and the
726 modified importin α-CaaX construct.
727 C) Confocal images of NF stage 42 *X. laevis* brains from *X. laevis* expressing an mCherry
728 construct modified with a c-terminal CaaX domain and grown in the presence of 100μM Wnt-
729 C59 immunostained for phospho-histone H3 and the modified CaaX construct.
730 D) Quantification of the number of phospho-histone H3 positive cells in stage 42 *X. laevis* brains
731 of *X. laevis* grown in the presence of DMSO or 100μM Wnt-C59 and expressing importin α-
732 CaaX or mCherry-CaaX. Wnt-C59 treated *X. laevis* embryos showed a significantly reduced
733 number of phospho-histone H3 positive cells in the brain compared to DMSO treated *X. laevis*.
734 *X. laevis* embryos expressing importin α-CaaX in the brain display a partial rescue of the
735 reduced phospho-histone H3 levels which was not recapitulated in *X. laevis* expressing mCherry-
736 CaaX. Mean +/- SEM n>10 *=p<0.05 ****=p<0.0001 determined by Student's t-test.
737

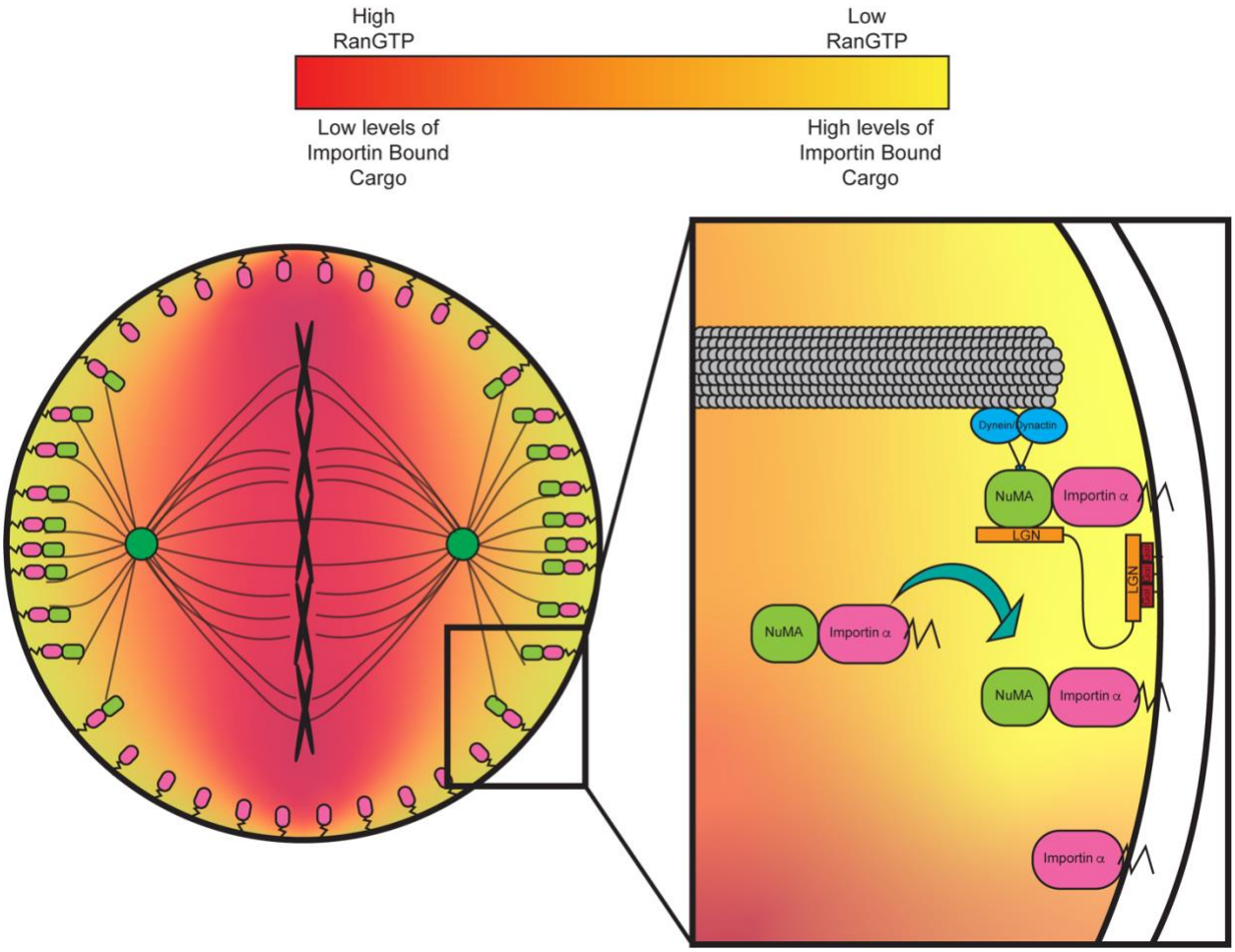

Figure 6. Importin α regulates mitotic spindle orientation through mediating NuMA localization to the metaphase cortex and maintenance at the cell cortex through anaphase in a palmitoylation dependent manner.

Proposed model of palmitoylated importin α's role in astral microtubule anchoring as a transporter of NuMA and a scaffold at the cell cortex for astral microtubule anchoring proteins to maintain cortical localization throughout metaphase and anaphase.

RESOURCE AVAILABILITY

Lead Contact for Reagent and Resource Sharing

Further information and requests for resources and reagents should be directed to and will be fulfilled by the Lead Contact, Christopher W. Brownlee (Christopher.Brownlee@stonybrook.edu).

Materials Availability

Plasmids generated in this study are being deposited to Addgene.

Data and Code Availability

- Microscopy data reported in this study will be shared by the lead contact upon request
- No original code was generated in this study
- Any additional information required to reanalyze the data reported in this paper is available from the lead contact upon request

MATERIALS AND METHODS

Reagents and Tools table

Reagent/Resource	Reference or Source	Identifier or Catalog Number
Experimental Models		
hTERT RPE-1 (human)	ATCC	CRL-4000
HCT 116 (human)	ATCC	CRL-4000
Xenopus laevis	NXR	N/A
Recombinant DNA		
Plasmid: Importin α-mCherry-CaaX	This study	N/A
Plasmid: Importin α-mCherry	This study	N/A
Plasmid: mCherry-CaaX	This study	N/A

Plasmid: Importin α-mCherry-CaaX (tet inducible)	This study	N/A
Plasmid: Importin α-mCherry (tet inducible)	This study	N/A
Plasmid: mCherry-CaaX (tet inducible)	This study	N/A
Plasmid: pcDNA6TR	Invitrogen T-Rex system from Thermofisher	Cat # V102520
Plasmid: pEGFP-C1-NuMA	Addgene	Cat # 81029
Plasmid: UBC::Importin α-mCherry-HA-CaaX	This study	N/A
Plasmid: UBC::Importin α-mCherry-HA-CaaX	This study	N/A
Antibodies		
Rabbit Polyclonal anti-NuMA	Novus Biologicals	Cat # NB100-74636
Rabbit Polyclonal anti-nestin	Sino Biological	Cat # 100244-T08
Monoclonal mouse living colors antibody	Takarabio	Cat # 632460
Rabbit polyclonal anti-mCherry	Proteintech	Cat # 26765-1-AP
Monoclonal mouse anti-importin α	Proteintech	Cat # 66870-1-Ig
Rabbit polyclonal anti-importin α	ABclonal	Cat # A1623
Monoclonal mouse anti-β tubulin	DSHB	Antibody E7
Monoclonal mouse anti-phospho histone H3	Proteintech	Cat # 66863-1-Ig
Monoclonal mouse anti-SAP97	Enzo Life Sciences	Cat # 06021547
Rabbit polyclonal anti-γ tubulin	Sigma-Aldrich	Cat # T5192
Monoclonal mouse anti-HA	Sigma-Aldrich	Cat # SAB2702196
Donkey anti-mouse IgG-AF488	Southern Biotech	Cat # 6411-30
Donkey anti-rabbit IgG-AF488	Southern Biotech	Cat # 6440-30

Donkey anti-mouse IgG-AF568	Invitrogen	Cat # A10037
Donkey anti-rabbit IgG-AF568	Invitrogen	Cat # A10042
Oligonucleotides and other sequence-based reagents		
Chemicals, Enzymes and other reagents		
Palmostatin-B	Sigma-Aldrich	Cat # 178501-5MG
Wnt-C59	Selleck Chem	Cat # S7037
Importazole	Selleck Chem	Cat # S8446
Ivermectin	ThermoFisher	Cat # J6277.03
2-BromoPalmitate	Sigma-Aldrich	Cat # 21604-1G
MG-132	Abcam	Cat # Ab141003
RO-3306	VWR International	Cat # 102516-266
McCoy's 5A Media	Avantor Scientific	Cat # 45000-374
Fetal bovine serum (FBS)	Avantor Scientific	Cat # 76327-086
PBS	Avantor Scientific	Cat # 45000-446
Gentamycin	Avantor Scientific	Cat # 102614-744
Duolink® *In Situ* Detection Reagents Red	Sigma-Aldrich	Cat # DUO92008
SE cell line 4D nucleofector X kit S	Lonza Bioscience	Cat # V4XC-1032
Software		
Celleste image analysis software version 6.0	Invitrogen	Cat # AMEP4942
Other		
Lonza 4D Nucleofector X-unit	Lonza Bioscience	Cat # AAF-1003X

Methods and Protocols

Cell culture

766 RPE-1 and HCT116 cells were cultured as previously described (Kiyomitsu and Cheeseman,
767 2012).

768 **Animal models**

769 Adult Female XLA.NXR-WTNXR (NXR_0031) frogs were purchased from the National
770 Xenopus Resource and maintained at the Stony Brook University animal facility. Frogs were
771 maintained in a pathogen-free facility held at 18°C, housed socially in aquatic tanks under
772 12:12h light:dark cycles and fed three times weekly with a pelleted Xenopus diet. All
773 experimental procedures were approved by the Institutional Animal Care and Use Committee.
774 All animals were maintained in accordance with standards established by the Division of
775 Laboratory Animal Resources at Stony Brook University

776

777 **Cell culture and immunostaining**

778 RPE-1 and HCT116 cells were cultured as previously described (Kiyomitsu and Cheeseman,
779 2012) in DMEM F-12 and McCoy's 5A media, respectively, supplemented with 5% FBS and
780 grown at 5% CO_2. Immunostaining was carried out on cells cultured onto fibronectin coated
781 coverslips, fixed with 4% PFA, permeabilized with PBS+0.2% Triton X-100 (Sigma-Aldrich
782 9036-19-5), and blocked with Bovine Serum Albumin (BSA) in PBS+0.2% Triton X-100. The
783 coverslips were than incubated with antibodies diluted in PBS+0.2% Triton X-100 as follows:
784 Rabbit polyclonal anti-NuMA 1:1000 (Novus Biologicals), monoclonal living colors antibody
785 1:1000 (Takarabio), rabbit polyclonal anti-mcherry 1:1000 (Proteintech), monoclonal anti-
786 importin α 1:1000 (Proteintech), rabbit polyclonal anti-importin α 1:1000 (ABclonal),
787 monoclonal anti-β tubulin E7 1:1000 (DSHB), monoclonal anti-SAP97 1:1000 (Enzo Life
788 Sciences), rabbit polyclonal anti-γ tubulin 1:1000 (Sigma-Aldrich), donkey anti-mouse IgG AF-

488 1:1000 (Southern Biotech), donkey anti-rabbit IgG AF-488 1:1000 (Southern Biotech), donkey anti-mouse IgG AF-568 1:1000 (Invitrogen) and donkey anti-rabbit IgG AF-488 1:1000 (Invitrogen). The coverslips were then mounted onto slides with ProLong Diamond Antifade Mountant (ThermoFisher P36961).

Mitotic arrest and drug treatment

RPE-1 and HCT116 cells were arrested in metaphase through a sequential drug treatment of RO-3306 and MG-132. Cells were treated with 9μM RO-3306 to arrest at the G2/M transition for 20 hours at 37°C. Cells were then washed with fresh media three times to remove RO-3306 and treated with 20μM MG-132 within 15 minutes of RO-3306 washout to arrest cells at metaphase. Cells were incubated in MG-132 for 1 hour at 37°C. In experiments with palmitoylation and importin function disrupting drug treatments cells were treated with DMSO, 10μM Wnt-C59, 50μM palmostatin, 40μM importazole, 25μM ivermectin, or 100μM 2-bromopalmitate with the MG-132 treatment and incubated for 1 hour at 37°C.

Spindle angle measurement

Mitotic spindle angles of metaphase-arrested cells were determined by measuring the vertical and horizontal distances between the centrosomes at each pole of the mitotic cell and calculating the arctangent of the vertical distance divided by the horizontal distance as follows:

$$\alpha = \arctan\left(\frac{z}{x}\right)$$

The vertical distance was determined through imaging the cell and measuring the length of a line drawn between each centrosome. The horizontal distance was determined through using a z-stack of the mitotic cell, determining at which z-slice each centrosome was in optimal focus, and calculating the z distance between each slice of optimal focus. Z-stacks were taken at a step distance of 0.1μm with varying numbers of steps depending on individual cell size.

812 ***X. laevis* fertilization**

813 *Xenopus laevis* adult females were induced to lay eggs by a priming injection of 100 U of
814 pregnant mare serum gonadotropin (PMSG) at least 48 hours before use and a boosting injection
815 of 500 U of human chorionic gonadotropin (hCG) 16 hours before use. Following the hCG
816 injection, adult female *X. laevis* were placed in a 2L water bath of 1X MMR (100 mM NaCl, 2
817 mM KCl, 1 mM $MgCl_2$, 2 mM $CaCl_2$, 0.1 mM EDTA, 5 mM HEPES pH 7.8) overnight at 17°C.
818 approximately 16 hours following hCG injection, fresh eggs were collected by squeezing eggs
819 from ovulating frogs into a 10cm plastic petri dish. To fertilize eggs, a sperm solution made from
820 ¼ of a male frog testis was placed in 1mL 1X MR (100 mM NaCl, 1.8 mM KCl, 2.0 mM $CaCl_2$,
821 1.0 $MgCl_2$, 5.0 mM HEPES-NaOH, pH 7.6) and homogenized using scissors and a pestle. 1mL
822 of sperm solution was added dropwise to the freshly squeezed eggs and the dish was swirled to
823 form a monolayer of eggs and incubated for 3 mins. Dishes were flooded with milli-Q water and
824 incubated for an additional 10 mins. Eggs were dejellied with a 2% cysteine solution for 6
825 minutes with occasional swirling and washed 5 times with 1/3 MR. Fertilized eggs were
826 incubated at 23°C until the appropriate developmental stage. In experiments where *X. laevis*
827 embryos were drug treated, the embryos were placed into a bath of 1/3 MR containing either
828 DMSO, 100µM Wnt-C59, or 1mM palmostatin 24 hours post fertilization and kept in drug bath
829 until the appropriate developmental stage for each experiment. In drug treatment conditions,
830 morphometric defects made it often difficult to determine the exact stage of Wnt-C59 and
831 palmostatin treated embryos between NF stages 40 to 43, so analysis was conducted when the
832 DMSO treated embryos were at the appropriate stage.

833 ***X. laevis* morphometric measurements**

834 *X. laevis* embryos were analyzed for morphometric defects at stage 42 by immobilizing embryos
835 in a bath of 140μg/mL MS-222 and imaging at 4X mounted upright. All measurements were
836 made in ImageJ. Distance between eyes was determined by measuring the straight line distance
837 from the right most portion of the left eye to the left most portion of the right eye, snout length
838 was determined by drawing a line from the front of the left eye to the right eye and then
839 measuring the straight line distance from the center of this line to the mouth, and overall head
840 area was determined by measuring the area of a circle drawn around the head such that each eye
841 is completely within the circle and the circle does not extend beyond the snout.

842 ***X. laevis* whole mount immunostaining**

843 *X. laevis* embryos were fixed in 4% PFA for 24 hours at 4°C. Following fixation, embryos were
844 immunostained by washing in PBS 3x20 min, photobleaching in a solution of 5% formamide and
845 1.2% hydrogen peroxide for 2 hours, washing in PBS + 0.1% Triton X-100 (PBST) overnight at
846 4°C, blocking with 2% BSA in PBST for 3 hours at RT, incubating with 1° antibodies diluted in
847 PBST overnight at 4°C as follows: rabbit polyclonal anti-nestin 1:1000 (Sino Biological), rabbit
848 polyclonal anti-mCherry 1:1000 (Proteintech), and monoclonal anti-phospho Histone H3 1:1000
849 (Proteintech), washing 3x1 hour in PBST, incubating with 2° antibodies diluted in PBST
850 overnight at 4°C as follows: , washing 3x1 hour in PBST and mounting onto a coverslip in
851 fluoromount G. In cases where embryos were cleared before mounting, embryos were chilled in
852 1-propanol and incubated 2x5 minutes, cleared with 5mL Murray's (2 parts Benzyl Benzoate and
853 1 part Benzyl Alcohol) and then mounted onto a coverslip with fluoromount G.

854 **Plasmid construct development**

855 Plasmid constructs were cloned into pCS2+ and pcDNA4TO vectors from existing plasmid
856 constructs of importin α, GFP, mCherry-CaaX, and NuMA-GFP.

857 **Embryo microinjection**

858 Plasmid was loaded into a needle pulled from a 1mm glass capillary tube (TW100F-3, World
859 Percision Instruments) using a L/M-3P-A electrode/needle puller. Embryos were placed in a
860 mesh-bottomed plastic dish with 2.5% Ficoll in 1/3 MR and microinjected with a 2nL droplet of
861 the appropriate plasmid using a Narishige IM-400 microinjector system equipped with a MM-3
862 micromanipulator (Narishige). For stage 1 injections embryos were injected directly at the
863 animal pole, for stage 2 injections 1 blastomere was injected at the animal pole, and for stage 5
864 injections the D11 blastomere was injected at roughly the middle of the blastomere (as per
865 Moody, 1987). pCS2+ plasmids were injected at a concentration of 10ng/μL such that the final
866 concentration of plasmid delivered was 20pg. pcDNA4TO plasmids were co-injected with
867 pcDNA6TR at concentrations of 5ng/μL and 25ng/μL respectively such that the final
868 concentration of total plasmid delivered was 60pg. Following injection, embryos were placed
869 into a new dish containing 2.5% Ficoll in 1/3 MR and incubated at 23ºC for 4 hours after which
870 embryos were moved to a dish containing 1/3 MR and incubated at 23ºC until appropriate
871 developmental stage. Embryos injected with pcDNA4TO + pcDNA6TR were placed in 1/3 MR
872 containing 12.5μg/mL doxycycline to induce gene expression 4 hours post injection and
873 transferred to fresh 1/3 MR with 12.5μg/mL doxycycline 24 hours post injection.

874 ***X. laevis* nestin positive cell count**

875 Stage 46 *X. laevis* embryos were whole mount fixed and stained for DNA (Hoechst) and nestin
876 (Rb α-nestin Sino Biological 100244-T08). Embryos were imaged at 20X magnification on an
877 EVOS M7000 epifluorescent microscope to generate a z-stack image of the brain of each
878 embryo. Z-stack images were processed in Celeste Image Analysis software for 3D-
879 deconvolution to remove background signal and using a parent child analysis measured the

880 number of DNA containing cells in the brain with overlapping nestin signal in the maximum
881 projection of the processed z-stack.

882 ***X. laevis* phospho-histone H3 positive cell count**

883 Stage 42 *X. laevis* embryos were whole mount fixed and stained for DNA (Hoechst), Phospho-
884 histone H3, and mCherry to visualize mCherry tagged proteins from microinjected constructs.
885 Whole embryos were imaged at 10X on a Zeiss LSM 980 confocal microscope by imaging a Z-
886 stack of the brain. A maximum projection image from this z-stack was then processed in Celeste
887 Image Analysis Software and a 3D count was measured in an ROI around the brain to determine
888 the number of cells positive for Phospho-histone H3 signal. Phospho-histone H3 positive cell
889 counts were determined by thresholding the minimal signal such that individual positive cells
890 could be resolved from background fluorescence.

891 **Proximity ligation assay**

892 Proximity ligation assay (PLA) was performed using DuoLink PLA (Millipore Sigma) following
893 the recommended protocol. PLA analysis of importin α and NuMA interaction was performed in
894 mitotically arrested HCT 116 cells using mouse anti-importin α (Proteintech) and rabbit anti-
895 NuMA (Novus Biologicals). PLA analysis of importin α and Dlg interaction was performed in
896 mitotically arrested HCT 116 cells using rabbit anti-importin α (ABclonal) and mouse anti-
897 SAP97 (Enzo Life Sciences). Cells were imaged with an EVOS M7000 epifluorescent
898 microscope at 60X magnification. Localization of PLA fluorescent signal was quantified by
899 counting the number of foci within three separate ROIs of each cell. Polar cortex ROI was
900 defined as the region from the plasma membrane at each pole to the centrosomes. Lateral cortex
901 ROI was defined as the region from the plasma membrane to the chromatin between the
902 centrosomes. Cytosol ROI was defined as the region between the centrosomes excluding the

903 plasma membrane. The number of foci in each region was calculated as a percentage of the total
904 number of foci for that cell. Cell border was determined by a brightfield image of each mitotic
905 cell quantified.

906 **Cell lysis and western blot analysis**

907 Lysates of RPE-1 and HCT 116 cells were generated from 10cm dishes seeded with $1x10^6$ cells 2
908 days prior to lysis. Cells were collected by washing with ice cold PBS and scraping off the plate
909 into solution. Cells were spun at 100xg for 5 minutes, supernatant was aspirated and cells were
910 resuspended in 150µL RIPA buffer (150 mM sodium chloride, 1.0% Triton X-100, 0.5% sodium
911 deoxycholate, 0.1% SDS, 50 mM Tris, pH 8.0) supplemented with 10µg/mL each of leupeptin,
912 pepstatin and chymostatin (LPC) protease inhibitors. Resuspended cells were rocked at 4ºC for 1
913 hour and spun at 12,000 rpm for 20 minutes at 4ºC in an Eppendorf FA-45-24-11 rotor.
914 Supernatant containing cell lysate proteins was then mixed 1:1 with 2X laemlli buffer, boiled at
915 100ºC for 5 minutes and stored at -20ºC until use. Western blot analysis was performed on cell
916 lysates by running lysates through SDS-PAGE in a 7.5% or 5.0% Tris-glycine gel (dependent on
917 size of proteins being analyzed), transferring to a nitrocellulose membrane, and blotting for target
918 proteins. Western blot analysis for NuMA was performed with overnight transfer of SDS-PAGE
919 gel at 20V at 4ºC while all other proteins were performed with a transfer at 150V for 90 minutes
920 at room temperature.

921 **Co-Immuno precipitation**

922 Co-immunoprecipitation was performed with Thermo Fisher IgG conjugated magnetic
923 Dynabeads following recommended protocol. Cell lysates were generated for
924 immunoprecipitation experiments with previously stated cell lysis protocol using a non-

denaturing lysis buffer (20 mMTris HCl pH 8, 137 mM NaCl, 1% Triton X-100, 2 mM EDTA) in place of RIPA buffer.

Mitotic protein localization measurement

To determine changes to KPNA2 and NuMA localization in cultured cells upon drug treatment, cells were mounted onto fibronectin coated coverslips, arrested in metaphase, drug treated, washed with cytoskeletal buffer (100mM NaCl, 300mM Sucrose, 3mM MgCl2, 10mM PIPES, pH 6.9, supplemented with 250µL 1M EGTA and 250µL Triton X-100 per 50 mL immediately before use), fixed with 4% PFA, and immunostained for DNA and KPNA2/NuMA. For KPNA2 localization cells were imaged using an EVOS M7000 at 100X with cell boundaries determined using bright-field images. For NuMA localization cells were imaged using a Leica SP5 confocal at 40X. To determine the cellular localization of target protein in each drug condition, 60 mitotic cells were imaged per drug treatment and the fluorescent intensity of KPNA2 or NuMA signal was measured in ImageJ at three cellular locations. A 10 pixel wide and 50 pixel long line was drawn at one cortical pole, one lateral membrane, and along the midline of the cell and measured. In order to normalize variations in intensity from inconsistent immunostaining, these measurements were normalized to each other on a cell-by-cell basis by determining the ratio of polar vs lateral signal, polar vs cytosolic signal, and lateral vs cytosolic signal. In the cases where one cortical pole differed in intensity from the opposite cortical pole, the pole with the higher measure of intensity was used for data analysis (the same method was used when measuring the lateral poles).

DNA transfection

HCT116 cells were seeded onto fibronectin coated coverslips. The following day media was replaced with serum free media and a mixture of 1µg plasmid in 12µL polyethylenimine (PEI)

948 was added dropwise to cells. Cells were incubated in PEI mixture for 4 hours then media was
949 washed out and replaced with complete media and incubated overnight before fixation and
950 imaging.

951 **Subcellular fractionation**

952 HCT116 cells were seeded in a 10cm dish and incubated at 37ºC. Following 2 days of incubation
953 Cells were incubated with DMSO for 1 hour at 37ºC then lifted from dish with ice cold PBS and
954 a cell scraper. Collected cells were then fractionated using the Minute Plasma Membrane/Protein
955 Isolation and Cell Fractionation kit from Invent Biotechnologies following the recommended
956 protocol.

957 **DNA nucleofection**

958 HCT116 cells were transfected via nucleofection using LONZA SE cell line 4D-Nucleofector kit
959 (Catalog #V4XC-1032) following recommended protocol. Following nucleofection cells were
960 incubated for 24 hours before fixation and immunostaining for mitotic spindle angle analysis.

961 **Palmitoylation prediction**

962 GPS-Palm (Ning et al., 2021) was employed for detection of potential palmitoylated cysteines
963 within human KPNA2. Cysteines above a threshold score of >0.6 (specificity > 85% and
964 accuracy > 82%) were considered to be likely palmitoylated.

965 **Nuclear localization signal, cellular localization, and protein function prediction**

966 NucPred (Brameier et al., 2007) was used to determine which proteins in the human genome
967 contain potential NLS sequences. Any proteins above a threshold score of >0.63 (specificity >
968 71% and accuracy >53%) were considered potential NLS-sequence containing candidate
969 proteins. Proteins were then filtered to discard transmembrane proteins while retaining only
970 plasma membrane proteins, as identified by UniProt GO identifiers (Ashburner et al., 2000;

971 Aleksander et al., 2023). Proteins were then sorted by cellular localization and function using
972 GO enrichment analysis (Thomas et al., 2022).
973
974
975 **QUANTIFICATION AND STATISTICAL ANALYSIS**
976 All statistical analysis was performed in GraphPad Prism 10.0. Comparisons between datasets
977 was determined by a student's t-test unless otherwise stated. Graphs represent the mean value +/-
978 the SEM unless otherwise stated. *$p<0.05$ **$p<0.01$ ***$p<0.001$ ****$p<0.0001$ unless
979 otherwise stated.
980
981
982 **References**
983 Alam, S.M. 2018. Proximity Ligation Assay (PLA). *Curr Protoc Immunol*. 123.
984 doi:10.1002/cpim.58.Proximity.
985 Aleksander, S.A., J. Balhoff, S. Carbon, J.M. Cherry, H.J. Drabkin, D. Ebert, M. Feuermann, P.
986 Gaudet, N.L. Harris, D.P. Hill, R. Lee, H. Mi, S. Moxon, C.J. Mungall, A. Muruganugan, T.
987 Mushayahama, P.W. Sternberg, P.D. Thomas, K. Van Auken, J. Ramsey, D.A. Siegele,
988 R.L. Chisholm, P. Fey, M.C. Aspromonte, M.V. Nugnes, F. Quaglia, S. Tosatto, M. Giglio,
989 S. Nadendla, G. Antonazzo, H. Attrill, G. Dos Santos, S. Marygold, V. Strelets, C.J.
990 Tabone, J. Thurmond, P. Zhou, S.H. Ahmed, P. Asanitthong, D. Luna Buitrago, M.N.
991 Erdol, M.C. Gage, M. Ali Kadhum, K.Y.C. Li, M. Long, A. Michalak, A. Pesala, A.
992 Pritazahra, S.C.C. Saverimuttu, R. Su, K.E. Thurlow, R.C. Lovering, C. Logie, S.
993 Oliferenko, J. Blake, K. Christie, L. Corbani, M.E. Dolan, L. Ni, D. Sitnikov, C. Smith, A.
994 Cuzick, J. Seager, L. Cooper, J. Elser, P. Jaiswal, P. Gupta, S. Naithani, M. Lera-Ramirez,

995 K. Rutherford, V. Wood, J.L. De Pons, M.R. Dwinell, G.T. Hayman, M.L. Kaldunski, A.E.
996 Kwitek, S.J.F. Laulederkind, M.A. Tutaj, M. Vedi, S.J. Wang, P. D'Eustachio, L. Aimo, K.
997 Axelsen, A. Bridge, N. Hyka-Nouspikel, A. Morgat, S.R. Engel, K. Karra, S.R. Miyasato,
998 R.S. Nash, M.S. Skrzypek, S. Weng, E.D. Wong, E. Bakker, T.Z. Berardini, L. Reiser, A.
999 Auchincloss, G. Argoud-Puy, et al. 2023. The Gene Ontology knowledgebase in 2023.
1000 *Genetics*. 224:1–14. doi:10.1093/genetics/iyad031.
1001 Anjur-Dietrich, M.I., V. Gomez Hererra, R. Farhadifar, H. Wu, H. Merta, S. Bahmanyar, M.J.
1002 Shelley, and D.J. Needleman. 2024. Mechanics of spindle orientation in human mitotic cells
1003 is determined by pulling forces on astral microtubules and clustering of cortical dynein.
1004 *Dev. Cell*. doi:10.1016/j.devcel.2024.05.022.
1005 Ashburner, M., C.A. Ball, J.A. Blake, D. Botstein, H. Butler, J.M. Cherry, A.P. Davis, K.
1006 Dolinski, S.S. Dwight, J.T. Eppig, M.A. Harris, D.P. Hill, L.I.-T.A. Kasarskis, S. Lewis,
1007 J.C. Matese, J.E. Richardson, M. Ringwald, G.M. Rubin, and G. Sherlock. 2000. Gene
1008 Ontology: tool for the unification of biology. *Nat. Genet.* 25:25–29.
1009 doi:10.2174/1381612824666180522105202.
1010 Bergstralh, D.T., N.S. Dawney, and D. St Johnston. 2017. Spindle orientation: A question of
1011 complex positioning. *Dev.* 144:1137–1145. doi:10.1242/dev.140764.
1012 Bergstralh, D.T., H.E. Lovegrove, I. Kujawiak, N.S. Dawney, J. Zhu, S. Cooper, R. Zhang, and
1013 D.S. Johnston. 2016. Pins is not required for spindle orientation in the drosophila wing disc.
1014 *Dev.* 143:2573–2581. doi:10.1242/dev.135475.
1015 Bergstralh, D.T., and D. St Johnston. 2014. Spindle orientation: What if it goes wrong? *Semin.*
1016 *Cell Dev. Biol.* 34:140–145. doi:10.1016/j.semcdb.2014.06.014.
1017 Bowman, S.K., R.A. Neumüller, M. Novatchkova, Q. Du, and J.A. Knoblich. 2006. The

1018 Drosophila NuMA Homolog Mud Regulates Spindle Orientation in Asymmetric Cell
1019 Division. *Dev. Cell*. 10:731–742. doi:10.1016/j.devcel.2006.05.005.
1020 Brameier, M., A. Krings, and R.M. MacCallum. 2007. NucPred - Predicting nuclear localization
1021 of proteins. *Bioinformatics*. 23:1159–1160. doi:10.1093/bioinformatics/btm066.
1022 Brownlee, C., and R. Heald. 2019. Importin α Partitioning to the Plasma Membrane Regulates
1023 Intracellular Scaling. *Cell*. 176:805-815.e8. doi:10.1016/j.cell.2018.12.001.
1024 Camuglia, J., S. Chanet, and A.C. Martin. 2022. Morphogenetic forces planar polarize LGN/Pins
1025 in the embryonic head during Drosophila gastrulation. *bioRxiv*. 2022.01.07.475359.
1026 Carvalho, C.A., S. Moreira, G. Ventura, C.E. Sunkel, and E. Morais-De-Sá. 2015. Aurora a
1027 triggers Lgl cortical release during symmetric division to control planar spindle orientation.
1028 *Curr. Biol.* 25:53–60. doi:10.1016/j.cub.2014.10.053.
1029 Chang, C.C., T.L. Huang, Y. Shimamoto, S.Y. Tsai, and K.C. Hsia. 2017. Regulation of mitotic
1030 spindle assembly factor NuMA by Importin-β. *J. Cell Biol.* 216:3453–3462.
1031 doi:10.1083/jcb.201705168.
1032 Charnley, M., F. Anderegg, R. Holtackers, M. Textor, and P. Meraldi. 2013. Effect of Cell Shape
1033 and Dimensionality on Spindle Orientation and Mitotic Timing. *PLoS One*. 8.
1034 doi:10.1371/journal.pone.0066918.
1035 Chhabra, S.N., and B.W. Booth. 2021. Asymmetric cell division of mammary stem cells. *Cell*
1036 *Div.* 16:1–15. doi:10.1186/s13008-021-00073-w.
1037 Dekker, F.J., O. Rocks, N. Vartak, S. Menninger, C. Hedberg, R. Balamurugan, S. Wetzel, S.
1038 Renner, M. Gerauer, B. Schölermann, M. Rusch, J.W. Kramer, D. Rauh, G.W. Coates, L.
1039 Brunsveld, P.I.H. Bastiaens, and H. Waldmann. 2010. Small-molecule inhibition of APT1
1040 affects Ras localization and signaling. *Nat. Chem. Biol.* 6:449–456.

1041 doi:10.1038/nchembio.362.
1042 Du, Q., and I.G. Macara. 2004. Mammalian Pins is a conformational switch that links NuMA to
1043 heterotrimeric G proteins. *Cell*. 119:503–516. doi:10.1016/j.cell.2004.10.028.
1044 Elmaci, I., M.A. Altinoz, R. Sari, and F.H. Bolukbasi. 2018. Phosphorylated Histone H3 (PHH3)
1045 as a Novel Cell Proliferation Marker and Prognosticator for Meningeal Tumors: A Short
1046 Review. *Appl. Immunohistochem. Mol. Morphol.* 26:627–631.
1047 doi:10.1097/PAI.0000000000000499.
1048 Ems-McClung, S.C., M. Emch, S. Zhang, S. Mahnoor, L.N. Weaver, and C.E. Walczak. 2020.
1049 RanGTP induces an effector gradient of XCTK2 and importin α/β for spindle microtubule
1050 cross-linking. *J. Cell Biol.* 219:1–15. doi:10.1083/jcb.201906045.
1051 Exner, C.R.T., and H.R. Willsey. 2021. Xenopus leads the way: Frogs as a pioneering model to
1052 understand the human brain. *Genesis*. 59. doi:10.1002/dvg.23405.
1053 Fankhaenel, M., F. Sadat Golestan Hashemi, M. Mosa Hosawi, L. Mourao, P. Skipp, X. Morin,
1054 C. LGJ Scheele, and S. Elias. 2023. Annexin A1 is a polarity cue that directs planar mitotic
1055 spindle orientation during mammalian epithelial morphogenesis. *bioRxiv*. 454117.
1056 doi:10.1038/s41467-023-35881-x.
1057 Finegan, T.M., and D.T. Bergstralh. 2019. Division orientation: disentangling shape and
1058 mechanical forces. *Cell Cycle*. 18:1187–1198. doi:10.1080/15384101.2019.1617006.
1059 Gallini, S., M. Carminati, F. De Mattia, I.A. Asteriti, and G. Guarguaglini. 2016. NuMA
1060 Phosphorylation by Aurora-A Orchestrates Spindle Orientation. *Curr. Biol.* 26:458–469.
1061 doi:10.1016/j.cub.2015.12.051.
1062 Goldfarb, D.S., A.H. Corbett, D.A. Mason, M.T. Harreman, and S.A. Adam. 2004. Importin α: A
1063 multipurpose nuclear-transport receptor. *Trends Cell Biol.* 14:505–514.

1064 doi:10.1016/j.tcb.2004.07.016.

1065 Guan, X., and C.A. Fierke. 2011. Understanding protein palmitoylation: Biological significance
1066 and enzymology. *Sci. China Chem.* 54:1888–1897. doi:10.1007/s11426-011-4428-2.

1067 Guo, L., K.S. Mohd, H. Ren, G. Xin, Q. Jiang, P.R. Clarke, and C. Zhang. 2019. Phosphorylation
1068 of importin-α1 by CDK1-cyclin B1 controls mitotic spindle assembly. *J. Cell Sci.* 132.
1069 doi:10.1242/jcs.232314.

1070 He, S., J.P. Gillies, J.L. Zang, C.M. Córdoba-Beldad, I. Yamamoto, Y. Fujiwara, J. Grantham,
1071 M.E. DeSantis, and H. Shibuya. 2023. Distinct dynein complexes defined by DYNLRB1
1072 and DYNLRB2 regulate mitotic and male meiotic spindle bipolarity. *Nat. Commun.* 14:1–
1073 15. doi:10.1038/s41467-023-37370-7.

1074 Higgins, C.D., and B. Goldstein. 2010. Asymmetric cell division: A new way to divide
1075 unequally. *Curr. Biol.* 23:R1029–R1031. doi:10.1016/j.earlhumdev.2006.05.022.

1076 Kalab, P., and R. Heald. 2008. The RanGTP gradient - A GPS for the mitotic spindle. *J. Cell Sci.*
1077 121:1577–1586. doi:10.1242/jcs.005959.

1078 Kaláb, P., A. Pralle, E.Y. Isacoff, R. Heald, and K. Weis. 2006. Analysis of a RanGTP-regulated
1079 gradient in mitotic somatic cells. *Nature*. 440:697–701. doi:10.1038/nature04589.

1080 Kennedy, A.E., and A.J. Dickinson. 2014. Quantification of orofacial phenotypes in xenopus. *J.*
1081 *Vis. Exp.* 1–14. doi:10.3791/52062.

1082 Kiyomitsu, T., and S. Boerner. 2021. The Nuclear Mitotic Apparatus (NuMA) Protein: A Key
1083 Player for Nuclear Formation, Spindle Assembly, and Spindle Positioning. *Front. Cell Dev.*
1084 *Biol.* 9:1–12. doi:10.3389/fcell.2021.653801.

1085 Kiyomitsu, T., and I.M. Cheeseman. 2012. Chromosome-and spindle-pole-derived signals
1086 generate an intrinsic code for spindle position and orientation. *Nat. Cell Biol.* 14:311–317.

1087 doi:10.1038/ncb2440.
1088 Kiyomitsu, T., and I.M. Cheeseman. 2013. XCortical dynein and asymmetric membrane
1089 elongation coordinately position the spindle in anaphase. *Cell*. 154:391.
1090 doi:10.1016/j.cell.2013.06.010.
1091 Konno, D., G. Shioi, A. Shitamukai, A. Mori, H. Kiyonari, T. Miyata, and F. Matsuzaki. 2008.
1092 Neuroepithelial progenitors undergo LGN-dependent planar divisions to maintain self-
1093 renewability during mammalian neurogenesis. *Nat. Cell Biol.* 10:93–101.
1094 doi:10.1038/ncb1673.
1095 Kotak, S., C. Busso, and P. Gönczy. 2014. NuMA interacts with phosphoinositides and links the
1096 mitotic spindle with the plasma membrane. *EMBO J.* 33:1815–1830.
1097 doi:10.15252/embj.201488147.
1098 Kotak, S., and P. Gönczy. 2013. Mechanisms of spindle positioning: Cortical force generators in
1099 the limelight. *Curr. Opin. Cell Biol.* 25:741–748. doi:10.1016/j.ceb.2013.07.008.
1100 Lasser, M., B. Pratt, C. Monahan, S.W. Kim, and L.A. Lowery. 2019. The many faces of
1101 Xenopus: Xenopus laevisas a model system to study Wolf-Hirschhorn syndrome. *Front.*
1102 *Physiol.* 10:1–12. doi:10.3389/fphys.2019.00817.
1103 Lin, D.T.S., and E. Conibear. 2015. ABHD17 proteins are novel protein depalmitoylases that
1104 regulate N-Ras palmitate turnover and subcellular localization. *Elife*. 4:1–14.
1105 doi:10.7554/eLife.11306.
1106 Mariscal, J., T. Vagner, M. Kim, B. Zhou, A. Chin, M. Zandian, M.R. Freeman, S. You, A.
1107 Zijlstra, W. Yang, and D. Di Vizio. 2020. Comprehensive palmitoyl-proteomic analysis
1108 identifies distinct protein signatures for large and small cancer-derived extracellular
1109 vesicles. *J. Extracell. Vesicles*. 9. doi:10.1080/20013078.2020.1764192.

1110 Moody, S.A. 1987a. Fates of the blastomeres of the 16-cell stage Xenopus embryo. *Dev. Biol.*
1111 119:560–578. doi:10.1016/0012-1606(87)90059-5.
1112 Moody, S.A. 1987b. Fates of the blastomeres of the 32-cell-stage Xenopus embryo. *Dev. Biol.*
1113 122:300–319. doi:10.1016/0012-1606(87)90296-X.
1114 Neville, K.E., T.M. Finegan, N. Lowe, P.M. Bellomio, D. Na, and D.T. Bergstralh. 2022. The
1115 Drosophila mitotic spindle orientation machinery requires activation, not just localization.
1116 *bioRxiv*.
1117 Ning, W., P. Jiang, Y. Guo, C. Wang, X. Tan, W. Zhang, D. Peng, and Y. Xue. 2021. GPS-Palm:
1118 A deep learning-based graphic presentation system for the prediction of S-palmitoylation
1119 sites in proteins. *Brief. Bioinform.* 22:1836–1847. doi:10.1093/bib/bbaa038.
1120 Oka, M., and Y. Yoneda. 2018. Importin α: Functions as a nuclear transport factor and beyond.
1121 *Proc. Japan Acad. Ser. B Phys. Biol. Sci.* 94:259–274. doi:10.2183/pjab.94.018.
1122 Okumura, M., T. Natsume, M.T. Kanemaki, and T. Kiyomitsu. 2018. Dynein–dynactin–NuMA
1123 clusters generate cortical spindle-pulling forces as a multiarm ensemble. *Elife*. 7:1–24.
1124 doi:10.7554/eLife.36559.
1125 Ozugergin, I., and A. Piekny. 2021. Complementary functions for the Ran gradient during
1126 division. *Small GTPases*. 12:177–187. doi:10.1080/21541248.2020.1725371.
1127 Pietro, F., A. Echard, and X. Morin. 2016. Regulation of mitotic spindle orientation: an
1128 integrated view. *EMBO Rep.* 17:1106–1130. doi:10.15252/embr.201642292.
1129 Pirovano, L., S. Culurgioni, M. Carminati, A. Alfieri, S. Monzani, V. Cecatiello, C. Gaddoni, F.
1130 Rizzelli, J. Foadi, S. Pasqualato, and M. Mapelli. 2019. Hexameric NuMA:LGN structures
1131 promote multivalent interactions required for planar epithelial divisions. *Nat. Commun.* 10.
1132 doi:10.1038/s41467-019-09999-w.

1133 Proffitt, K.D., B. Madan, Z. Ke, V. Pendharkar, L. Ding, M.A. Lee, R.N. Hannoush, and D.M.
1134 Virshup. 2013. Pharmacological inhibition of the Wnt acyltransferase PORCN prevents
1135 growth of WNT-driven mammary cancer. *Cancer Res.* 73:502–507. doi:10.1158/0008-
1136 5472.CAN-12-2258.
1137 Razuvaeva, A. V., L. Graziadio, V. Palumbo, G.A. Pavlova, J. V. Popova, A. V. Pindyurin, S.
1138 Bonaccorsi, M.P. Somma, and M. Gatti. 2023. The Multiple Mitotic Roles of the ASPM
1139 Orthologous Proteins: Insight into the Etiology of ASPM-Dependent Microcephaly. *Cells*.
1140 12:922. doi:10.3390/cells12060922.
1141 Saadaoui, M., M. Machicoane, F. di Pietro, F. Etoc, A. Echard, and X. Morin. 2014. Dlg1
1142 controls planar spindle orientation in the neuroepithelium through direct interaction with
1143 LGN. *J. Cell Biol.* 206:707–717. doi:10.1083/jcb.201405060.
1144 Schelar, E. and, and J. Liu. 2008. 基因的改变NIH Public Access. *Bone*. 23:1–7.
1145 doi:10.1038/nmeth.1293.Large-Scale.
1146 Schiller, E.A., and D.T. Bergstralh. 2021. Interaction between Discs large and
1147 Pins/LGN/GPSM2: a comparison across species. *Biol. Open*. 10:1–10.
1148 doi:10.1242/bio.058982.
1149 Seldin, L., N.D. Poulson, H.P. Foote, and T. Lechler. 2013. NuMA localization, stability, and
1150 function in spindle orientation involve 4.1 and Cdk1 interactions. *Mol. Biol. Cell*. 24:3651–
1151 3662. doi:10.1091/mbc.E13-05-0277.
1152 Serwa, R.A., F. Abaitua, E. Krause, E.W. Tate, and P. O'Hare. 2015. Systems Analysis of
1153 Protein Fatty Acylation in Herpes Simplex Virus-Infected Cells Using Chemical
1154 Proteomics. *Chem. Biol.* 22:1008–1017. doi:10.1016/j.chembiol.2015.06.024.
1155 Shantanam, S., and MUELLER. 2018. Modeling human craniofacial disorders in Xenopus.

1156 *Physiol. Behav.* 176:139–148. doi:10.1007/s40139-017-0128-8.Modeling.

1157 Singh, D., N. Schmidt, F. Müller, T. Bange, and A.W. Bird. 2021. Destabilization of Long Astral
1158 Microtubules via Cdk1-Dependent Removal of GTSE1 from Their Plus Ends Facilitates
1159 Prometaphase Spindle Orientation. *Curr. Biol.* 31:766-781.e8.
1160 doi:10.1016/j.cub.2020.11.040.

1161 Sobocinska, J., P. Roszczenko-Jasinska, M. Zareba-Kozio, A. Hromada-Judycka, O. V.
1162 Matveichuk, G. Traczyk, K. Ukasiuk, and K. Kwiatkowska. 2018. Lipopolysaccharide
1163 Upregulates Palmitoylated Enzymes of the Phosphatidylinositol Cycle: An Insight from
1164 Proteomic Studies. *Mol. Cell. Proteomics*. 17:233–254. doi:10.1074/mcp.RA117.000050.

1165 Soderholm, J.F., S.L. Bird, P. Kalab, Y. Sampathkumar, K. Hasegawa, M. Uehara-Bingen, K.
1166 Weis, and R. Heald. 2011. Importazole, a small molecule inhibitor of the transport receptor
1167 importin-β. *ACS Chem Biol*. 6:700–708. doi:10.1016/j.earlhumdev.2006.05.022.

1168 Stooke-Vaughan, G.A., L.A. Davidson, and S. Woolner. 2017. Xenopus as a model for studies in
1169 mechanical stress and cell division. *Genesis*. 55. doi:10.1002/dvg.23004.

1170 Suzuki, S., J. Namiki, S. Shibata, Y. Mastuzaki, and H. Okano. 2010. The neural stem/progenitor
1171 cell marker nestin is expressed in proliferative endothelial cells, but not in mature
1172 vasculature. *J. Histochem. Cytochem.* 58:721–730. doi:10.1369/jhc.2010.955609.

1173 Takeda, E., T. Murakami, G. Matsuda, H. Murakami, T. Zako, M. Maeda, and Y. Aida. 2011.
1174 Nuclear exportin receptor cas regulates the NPI-1-mediated nuclear import of HIV-1 vpr.
1175 *PLoS One*. 6. doi:10.1371/journal.pone.0027815.

1176 Tamanoi, F., C.L. Gau, C. Jiang, H. Edamatsu, and J. Kato-Stankiewicz. 2001. Protein
1177 farnesylation in mammalian cells: Effects of farnesyltransferase inhibitors on cancer cells.
1178 *Cell. Mol. Life Sci.* 58:1636–1649. doi:10.1007/PL00000802.

1179 Tang, X., J.J. Punch, and W.L. Lee. 2009. A CAAX motif can compensate for the PH domain of
1180 Num1 for cortical dynein attachment. *Cell Cycle*. 8:3182–3190. doi:10.4161/cc.8.19.9731.
1181 Tarannum, N., R. Singh, and S. Woolner. 2022. Sculpting an Embryo: The Interplay between
1182 Mechanical Force and Cell Division. *J. Dev. Biol.* 10. doi:10.3390/jdb10030037.
1183 Taverna, E., M. Götz, and W.B. Huttner. 2014. The cell biology of neurogenesis: toward an
1184 understanding of the development and evolution of the neocortex. 30. 465–502 pp.
1185 Thinon, E., J.P. Fernandez, H. Molina, and H.C. Hang. 2018. Selective Enrichment and Direct
1186 Analysis of Protein S-Palmitoylation Sites. *J. Proteome Res.* 17:1907–1922.
1187 doi:10.1021/acs.jproteome.8b00002.
1188 Thomas, P.D., D. Ebert, A. Muruganujan, T. Mushayahama, L.P. Albou, and H. Mi. 2022.
1189 PANTHER: Making genome-scale phylogenetics accessible to all. *Protein Sci.* 31:8–22.
1190 doi:10.1002/pro.4218.
1191 Toyoshima, F., and E. Nishida. 2007. Integrin-mediated adhesion orients the spindle parallel to
1192 the substratum in an EB1- and myosin X-dependent manner. *EMBO J.* 26:1487–1498.
1193 doi:10.1038/sj.emboj.7601599.
1194 Tsuchiya, K., H. Hayashi, M. Nishina, M. Okumura, Y. Sato, M.T. Kanemaki, G. Goshima, and
1195 T. Kiyomitsu. 2021. Ran-GTP Is Non-essential to Activate NuMA for Mitotic Spindle-Pole
1196 Focusing but Dynamically Polarizes HURP Near Chromosomes. *Curr. Biol.* 31:115-127.e3.
1197 doi:10.1016/j.cub.2020.09.091.
1198 Wagstaff, K.M., H. Sivakumaran, S.M. Heaton, D. Harrich, and D.A. Jans. 2012. Ivermectin is a
1199 specific inhibitor of importin α/β-mediated nuclear import able to inhibit replication of
1200 HIV-1 and dengue virus. *Biochem. J.* 443:851–856. doi:10.1042/BJ20120150.
1201 Weaver, L.N., and C.E. Walczak. 2015. Spatial gradients controlling spindle assembly. *Biochem.*

1202 *Soc. Trans.* 43:7–12. doi:10.1042/BST20140243.

1203 Won, S.J., and B.R. Martin. 2018. Temporal Profiling Establishes a Dynamic S-Palmitoylation
1204 Cycle. *ACS Chem. Biol.* 13:1560–1568. doi:10.1021/acschembio.8b00157.

1205 Yang, Y., M. Liu, D. Li, J. Ran, J. Gao, S. Suo, S. Sun-Cong, and J. Zhou. 2014. CYLD
1206 regulates spindle orientation by stabilizing astral microtubules and promoting dishevelled-
1207 NuMA-dynein/ dynactin complex formation. *Proc. Natl. Acad. Sci. U. S. A.* 111:2158–
1208 2163. doi:10.1073/pnas.1319341111.

1209 Yu, F., X. Morin, Y. Cai, X. Yang, and W. Chia. 2000. Analysis of partner of inscuteable, a
1210 novel player of Drosophila asymmetric divisions, reveals two distinct steps in inscuteable
1211 apical localization. *Cell*. 100:399–409. doi:10.1016/S0092-8674(00)80676-5.

1212 Yu, M., K. Qin, J. Fan, G. Zhao, P. Zhao, W. Zeng, C. Chen, A. Wang, Y. Wang, J. Zhong, Y.
1213 Zhu, W. Wagstaff, R.C. Haydon, H.H. Luu, S. Ho, M.J. Lee, J. Strelzow, R.R. Reid, and
1214 T.C. He. 2024. The evolving roles of Wnt signaling in stem cell proliferation and
1215 differentiation, the development of human diseases, and therapeutic opportunities. *Genes*
1216 *Dis.* 11:101026. doi:10.1016/j.gendis.2023.04.042.

1217 Zheng, Z., Q. Wan, J. Liu, H. Zhu, X. Chu, and Q. Du. 2013. Evidence for dynein and astral
1218 microtubule-mediated cortical release and transport of Gαi/LGN/NuMA complex in mitotic
1219 cells. *Mol. Biol. Cell*. 24:901–913. doi:10.1091/mbc.E12-06-0458.

1220 Zhong, T., X. Gongye, M. Wang, and J. Yu. 2022. Understanding the underlying mechanisms
1221 governing spindle orientation : How far are we from there ? 1–7. doi:10.1111/jcmm.17526.

1222 Zhou, B., Y. Wang, Y. Yan, J. Mariscal, D. Di Vizio, M.R. Freeman, and W. Yang. 2019. Low-
1223 background acyl-biotinyl exchange largely eliminates the coisolation of non- s-acylated
1224 proteins and enables deep s-acylproteomic analysis. *Anal. Chem.* 91:9858–9866.

1225 doi:10.1021/acs.analchem.9b01520.

1226 Zhou, C.Y., B. Dekker, Z. Liu, H. Cabrera, J. Ryan, J. Dekker, and R. Heald. 2023. Mitotic

1227 chromosomes scale to nuclear-cytoplasmic ratio and cell size in xenopus. *Elife*. 12.

1228 doi:10.7554/eLife.84360.

1229